How have Divergent Global Emission Trends Influenced Long-range Transported Ozone to North America?

Rohit Mathur[1*], Daiwen Kang[1], Sergey L. Napelenok[1], Jia Xing[2], Christian Hogrefe[1], Golam Sarwar[1], Syuichi Itahashi[3], Barron H. Henderson[4]

[1] Center for Environmental Measurement and Modeling, Office of Research and Development, U.S. Environmental Protection Agency, RTP, NC, USA

[2] Tsinghua University, Beijing, China

[3] Environmental Science Research Laboratory, Central Research Institute of Electric Power Industry (CRIEPI), Japan

[4] Office of Air Quality Planning and Standards, U.S. Environmental Protection Agency, RTP, NC, USA

[*]*Correspondence to*: Rohit Mathur (mathur.rohit@epa.gov)

Key Points

- Changes in global emission patterns have and continue to alter long-range transport and background O_3 air pollution levels
- Long-range transported O_3 to North America has a prominent contribution from open sea shipping emissions and needs improved quantification
- Stratospheric O_3 (ranging between 6-20ppb) constitutes 29-78% of the estimated Spring-time background O_3 across the continental U.S.

Abstract: Several locations across the United States in non-compliance with the national standard for ground-level ozone (O_3) are thought to have sizeable influences from distant extra-regional emission sources or natural stratospheric O_3, which complicates design of local emission control measures. To quantify the amount of long-range transported O_3 (LRT O_3), its origin, and change over time, we conduct and analyze detailed sensitivity calculations characterizing the response of O_3 to emissions from different source regions across the Northern Hemisphere in conjunction with multi-decadal simulations of tropospheric O_3 distributions and changes. Model calculations show that the amount of O_3 at any location attributable to sources outside North America varies both spatially and seasonally. On a seasonal-mean basis, during 1990-2010, LRT O_3 attributable to international sources steadily increased by 0.06-0.2 ppb yr^{-1} at locations across the United States and arose from superposition of unequal and contrasting trends in individual source-region contributions, which help inform attribution of the trend evident in O_3 measurements. Contributions of emissions from Europe steadily declined through 2010, while those from Asian emissions increased and remained dominant. Steadily rising NO_x emissions from international shipping resulted in increasing contributions to LRT O_3, comparable to those from Asian emissions in recent years. Central American emissions

contribute a significant fraction of LRT O_3 in southwestern United States. In addition to the LRT O_3 attributable to emissions outside of North America, background O_3 across the continental United States is comprised of a sizeable and spatially variable fraction that is of stratospheric origin (29-78%).

Plain Language Summary Though implementation of control measures and technological advances have reduced ground-level ozone pollution across the United States, increasing amounts of ozone pollution inter-continentally transported from other world regions with increasing emissions, combined with changing and uncertain amounts of natural ozone from variability in stratosphere-troposphere exchange processes, can confound design and implementation of local air pollution abatement strategies. "Background" or amount not produced locally, constitutes a larger fraction of the ozone pollution at a location as local control measures are implemented. Detailed model calculations are analyzed to explain the role of the dominant source regions that drive the 1990-2010 changes noted in observed ground-level ozone measurements across the U.S. In recent years, the contributions of shipping emissions to ozone imported to the U.S. troposphere are comparable to those from transport of ozone attributable to East Asian emissions and could be higher in the future if commercial shipping operations were to increase in response to anticipated growth in seaborne trade. In addition to the O_3 attributable to emissions from different world regions, air-masses entering the North American domain have sizeable contributions of natural ozone of stratospheric origin, variability in which needs improved quantification to guide background ozone assessments and policy deliberations.

1. Introduction

Ground-level ozone (O_3) is a key air pollutant of concern due to its harmful effects on human health, vegetation, and crop yield (Lippman, 1993; Chameides et al., 1994; Krupa et al., 1998; U.S. EPA, 2020a). Though the chemistry of O_3 formation in the troposphere from its precursor oxides of nitrogen (NO_x) and volatile organic compounds (VOCs) has long been understood and studied (Haagen-Smit and Fox, 1954), clear attribution of its levels at a location is complicated by contributions from multiple sources including domestic and international anthropogenic precursor emissions as well as natural sources including lightning, soil, wildfires, biogenic emissions, and stratosphere-troposphere exchange (STE). Substantial progress has been achieved in reducing ground-level O_3 concentrations and consequent human and ecosystem exposure across the continental United States as a result of a combination of control measure implementation as well as technological advances that have significantly reduced emissions of NO_x and VOCs over the past three decades (U.S. EPA, 2020b), and is evident in numerous studies analyzing long-term trends in observed surface-level O_3 mixing ratios (e.g., Cooper et al., 2012, Simon et al, 2015, Xing et al., 2015; Mathur et al., 2018; Gaudel et al., 2018). Despite this progress, attainment of the O_3 National Ambient Air Quality Standard (NAAQS) continues to remain a challenge at many locations across the continental United States, with studies suggesting that a large fraction of the population is still exposed

to unhealthy levels of O_3 pollution (ALA, 2020) and recommending standards lower than the current NAAQS (e.g., Cromar et al., 2019). As measures to limit domestic emissions are implemented, the contributions of natural sources and increasing O_3 pollution transported from other regions become more influential in shaping local O_3 levels and confound implementation of abatement measures and design of emission strategies to meet more stringent NAAQS.

Strategies for reducing pollution levels in surface air over a region are complicated not only by the interplay of local emission sources and complex physical, chemical, dynamical processes in the atmosphere, but also by the hemispheric background levels of pollutants (NRC, 2009; TFHTAP, 2010). Previous analyses of long-term observations of ground-level O_3 have shown distinct regional and seasonal trends across the measured O_3 concentration distributions. While ground-level O_3 has generally declined at non-urban locations across the eastern United States, many locations in the western United States and at higher elevations indicate increasing trends in the lower O_3 percentiles measured at least through 2010 (Lin et al., 2000; Jaffe et al., 2003; Cooper et al., 2012). This increase is suggestive of increasing O_3 flowing into the western United States, which has been linked to rising amounts of long-range transported Asian pollution that reach the lower free troposphere and surface of the western United States (Jacob et al., 1999; Jaffe et al., 1999; Parish et al., 2004; Lin et al., 2017). However, the paucity of long-term records to characterize changes in O_3 and precursor species aloft in the atmosphere, where transport is efficient, make it difficult to accurately attribute the noted changes in surface O_3 to distant sources and the space and time variations in their contributions (cf. Mathur et al., 2018).

Large and contrasting changes in emission patterns across the globe (e.g. declining emissions in North America and Western Europe in response to implementation of control measures and increasing emissions across Asia, Central America, and Eastern Europe due to economic and population growth) have and continue to result in heterogeneous changes in the tropospheric chemical composition (e.g., Xing et al., 2015), and are likely altering long-range transport, and consequently impacting background pollution levels at receptor regions. Fiore et al. (2009) examined intercontinental source-receptor relationships for O_3 pollution using simulations from multiple models that simulated impacts of a fixed emission perturbation from four continental-scale northern midlatitude source regions on surface O_3 levels in the same regions. Their results illustrate that air pollution levels in any receptor region are influenced by emissions originating in multiple source regions, thereby suggesting that both the impacts of changes in emissions in the individual source regions and potential benefits of emission reductions are likely unevenly distributed across multiple receptor regions. Thus, understanding the space and time contributions of long-range transported O_3 (LRT O_3) pollution, its attribution to various source regions, and the possible changes in such attribution over time is important for guiding development of future national and local air pollution abatement strategies.

To shed light on these issues and better understand the contributions of different source regions across the Northern Hemisphere to long-range transported O_3 to North America, we exercise a detailed sensitivity analysis method in the Hemispheric Community Multiscale Air Quality (HCMAQ) modeling system (Mathur et al., 2017), and analyze these in conjunction with long-term simulations for the 1990-2010 period to assess how regionally heterogeneous changes in NO_x and VOC emissions across the Northern Hemisphere influenced long-range transport of O_3 and the changing contributions of the source regions in response to emission changes during this multi-decadal time period. Conducting the analyses for a historical time-period, for which model predictions of atmospheric composition have been extensively evaluated relative to available observations in previous studies, provides greater confidence in the inferred source-region contributions and changes in long-range O_3 transport patterns.

1. Methodology

(a) Modeling System and Simulation Details

In this analysis, we combine detailed sensitivity calculations describing the response of tropospheric O_3 distributions to emissions from different regions with previously conducted multi-decadal simulations to characterize changes in tropospheric O_3 across the Northern Hemisphere during the period 1990-2010 (Xing et al., 2015). These simulations utilized the Community Multiscale Air Quality (CMAQ) version 5.0 (doi:10.5281/zenodo.1079888) extended for hemispheric applications (HCMAQ) (Mathur et al., 2017). The process configuration options used in the model calculations described here follow those detailed in Xing et al. (2015) and Mathur et al. (2017). Briefly, the horizontal domain covering the Northern Hemisphere set on a polar stereographic projection (see Figure 1) is discretized with a 187x187 grid of 108 km resolution. A terrain-following vertical coordinate utilizing 44 layers of variable thickness is used to resolve the model vertical extent between the surface and 50 hPa. To minimize interpolation error and to avoid introducing mass imbalances, hemispheric simulations with CMAQ inherit the projection and grid structure from the Weather Research and Forecasting (WRF) model, which provides the driving meteorological fields. The WRF simulations, in turn, were constrained by NCEP/NCAR Reanalysis data with a 2.5° spatial and 6-hour temporal resolution. WRF's simulation of hourly surface temperature, relative humidity, wind speed and direction have previously been evaluated by Xing et al. (2015) through comparison with observations and no significant bias in the meteorological fields were detected.

Year specific estimates of emissions over the Northern Hemisphere were derived from the EDGAR (Emission Database for Global Atmospheric Research, version 4.2; European Commission, 2011) database which reports emissions for 17 anthropogenic sectors and large-scale biomass burning on a $0.1° \times 0.1°$ resolution grid. Biogenic VOC (based on the MEGAN model; Guenther et al., 1995) and lightning NO_x (Price et al, 1997) emissions were obtained from GEIA (Global Emission Inventory Activity; http://www.geiacenter.org). Xing et al. (2015) further describe the processing of global emission inventories for CMAQ, includ-

ing temporalization of the annual estimates to hourly model inputs, vertical distributions of anthropogenic and lightning emissions, and speciation of fine particulate matter ($PM_{2.5}$) and non-methane volatile organic compounds (NMVOC) emissions to model primary aerosol constituents and gas-phase species. Emissions of nitric oxide (NO) from soil or sulfur dioxide (SO_2) from volcanos were not considered in the applications presented here.

The lateral boundaries of the hemispheric domain are in the area encircling the Earth near the equator where because of the presence of the intertropical convergence zone (ITCZ), the mixing of air masses originating in the Northern and Southern Hemispheres occurs relatively slowly. The chemical lateral boundary conditions were set to represent clean tropospheric conditions and as detailed in Mathur et al. (2017) their impacts are typically confined to the lower latitudes and do not propagate into the domain. CMAQ was configured to use the Carbon Bond 2005 chemical mechanisms with updated toluene chemistry (CB05TU) gas-phase chemistry mechanism with modifications to represent multi-day chemistry associated with cycling of NO_x through reservoir organic nitrate species as described in Mathur et al. (2017). These involved updating the rate constant for the organic nitrate reaction with hydroxyl radical (OH) to that for isoprene nitrates (since on the hemispheric scale organic nitrates formed from isoprene are the largest contributor to its simulated tropospheric budget), and enhancing its physical sinks via dry deposition and wet scavenging (since the Henry's law constants for several alkyl nitrates of biogenic emissions have been suggested to be higher than peroxyacetyl nitrate (PAN), e.g., Treves and Rudich (2003)). Additionally, to represent the impacts of STE on tropospheric O_3 distribution, we specify O_3 in the modelled upper troposphere/lower stratosphere (UTLS) based on estimated potential vorticity (PV). O_3 at the model top is specified by multiplying the space- and time-varying model-estimated PV in the top-most model layer with a scaling factor of 20 ppb/PV-unit based on previously developed UTLS O_3-PV correlations (Mathur et al., 2008). It should be noted that while both the treatment of organic nitrates and the approach to PV scaling have been significantly enhanced in recent versions of the CMAQ modeling system, using the two specific process configuration choices described above enable us to conduct detailed sensitivity calculations (discussed in next section) with a model configuration that matches the one used to create the 1990-2010 multi-decadal tropospheric composition time-series and combine these two sets of model calculations in a complementary manner to infer changes in long-range transport of O_3.

1. Sensitivity Analysis Method

The decoupled direct method in three-dimensions (DDM-3D), implemented in the CMAQ modeling system (Napelenok et al., 2008), is an efficient and accurate approach for probing the sensitivity of atmospheric pollutant concentrations to changes in model inputs and parameters. DDM is a formal mathematical method that uses direct derivates of equations governing the evolution of species concentrations in the atmosphere to calculate the local sensitivities

to a variety of model parameters and input data (Yang et al., 1997). Since the equations governing the sensitivity coefficients have a structure similar to that of the governing species conservation equation in CMAQ, the sensitivity coefficient calculations can elegantly follow, in a decoupled manner, the process parameterizations and numerical methods used to solve the governing equations for the species concentrations. Both first- and second-order sensitivity coefficients can be estimated using the current implementation of DDM-3D in CMAQ. The second order sensitivities help better capture non-linearities in the system (Hakami et al., 2003; Cohan and Napelenok, 2011), as would be useful in describing O_3 formation and evolution in plumes near-downwind of source regions.

The sensitivity analysis method enables one to examine the response of the modeled concentrations field to perturbations in modeled parameters. The perturbation to the parameter P_j (in the base case simulation) can be described as

$$\varepsilon_j P_j = \left(1 + \ \varepsilon_j\right) P_j = p_j \ (1)$$

where, $_j$ is a scaling factor and p_j is the perturbed sensitivity parameter. Following Napelenok et al. (2008), the semi-normalized first order sensitivity (S_j) of concentration of a species in response to perturbation in p_j can then be estimated by scaling to its nominal value, P_j, as

$$S_j = P_j \frac{\partial C}{\partial p_j} = P_j \frac{\partial C}{\partial (\varepsilon_j P_j)} = \frac{\partial C}{\partial \varepsilon_j} \ (2)$$

Note that S_j has the same units as concentrations and $_j$ is unitless. Combing Equation 2 with the governing species conservation equation in the model yields the governing equation for S_j analogous to that for the species concentrations; thus, the species sensitivity calculation can be propagated through all the same processes as for the species concentration, yielding a three-dimensional species sensitivity field (Hakami et al., 2003; Napelenok et al., 2008; Cohan and Napelenok, 2011). Projecting the fractional perturbations from the base case simulations, the perturbed concentrations can be approximated using the Taylor series expansion:

$$C_{\text{perturb}} \approx C_{\text{base}} + S_j \ \varepsilon_j + h.o.t \ (3)$$

where, h.o.t represents second and higher order terms. Finally, a zero-out contribution (ZOC), defined as the difference between the base-case simulation and the concentration that would occur if the sensitivity parameter did not exist (i.e., $p_j = 0$ or $_j = 1$) can be approximated as (Cohan et al., 2005)

$$ZOC = \ C_{\text{base}} - C_{p_j=0} \ \approx \ S_j \ (4)$$

We use the DDM-3D approach to estimate sensitivity of simulated three-dimensional tropospheric O_3 to emissions from different source regions across the Northern Hemisphere. We adopt the TFHTAP definitions of these source regions from Galmarini et al. (2017) but group them to larger geographic regions. Since O_3 production is dependent on both NO_x and VOC emissions, calculating both first and second order sensitivity coefficients for O_3 to both

precursors and for each source region for extended simulation periods becomes computationally prohibitive. Thus, to examine the sensitivity of tropospheric O_3 across the Northern Hemisphere across different seasons, we grouped the source regions and also tracked only the first order sensitivities to NO_x and VOC emissions from these regions over an entire annual cycle for the 2006 calendar year. Additionally, to more accurately project the sensitivities to other emission perturbation years while balancing the computational constraints, we also calculated second-order sensitivities only to global NO_x and VOC emissions for the 2006 calendar year. Since our primary focus is to characterize the influence of different world regions on tropospheric O_3 and the long-range transported amounts to North America, we focus on sensitivity to total NO_x and VOC emissions from the regions and do not distinguish between anthropogenic and biogenic components of the contribution. It should also be noted that the sensitivity to VOC emissions from a region includes both NMVOC and carbon monoxide (CO). Though the contributions of CO to O_3 formation are comparatively small, its inclusion with the VOC sensitivity fully completes all O_3 precursors as they are identified in the chemical mechanism. Our previous analyses of DDM-3D calculations across the Northern Hemisphere (Itahashi et al., 2020b) show that the values of sensitivity coefficients to VOC emissions are small compared to those to NO_x emissions, and that the second-order sensitivity coefficients of O_3 to VOC emissions are even smaller. This suggests that the nonlinear response of large-scale O_3 distributions to VOC emissions is negligible and that O_3 over the midlatitude Northern Hemisphere is in a NO_x-sensitive regime. Also, as illustrated in Section S2 of the supporting information, the estimated far field impacts of long-range pollution transport discussed in subsequent analysis is not impacted by our choice of not propagating higher-order sensitivity coefficients for each source region. We thus expect minimal impact of the simplifications in our simulation experiment design on the analysis presented here.

The entire Northern Hemisphere modeling domain was divided into seven source regions (see Figure 1) nominally representing: (1) North America (NAM), (2) Europe including all of Russia (EUR+RUS), (3) East and Southeast Asia (EAS+SEA), (4) South Asia (SAS; the Indian subcontinent), (5) Northern Africa and the Middle East (NAF+MDE), (6) Central America (CAM), and (7) Other (the rest of the geographic domain including the vast oceanic regions). In addition, the sensitivity of simulated three-dimensional O_3 to the O_3 specified in the top-most layer as a function of the space and time varying PV fields was also tracked. Since this PV-scaled O_3 at the model top is representative of STE, this sensitivity can be interpreted to represent the modeled O_3 that is of stratospheric origin. To minimize the impact of short-term meteorological variability on inferred long-range transport, in subsequent analyses we focus on seasonal-averaged values of the sensitivity coefficient which in turn were derived from the hourly model output values. Note that 2006 was chosen as the base year for the DDM-3D annual simulations based on previous applications and evaluation of the H-CMAQ modeling system for this calendar year (e.g.,

Xing et al., 2016; Mathur et al., 2017).

1. Results and Discussion

The CMAQ model configured with DDM-3D (Napelenok et al., 2008) as described in Section 2 was exercised over an annual cycle for the base year 2006 to estimate the sensitivity of O_3 to NO_x and VOC emissions from each of the seven geographic source regions and the sensitivity of O_3 to STE influences. In subsequent discussion, $S_{NOx,j}$ and $S_{VOC,j}$ represent the first order sensitivity of modeled O_3 to NO_x and VOC emissions from source region j, and $S^2_{NOx,G}$ and $S^2_{VOC,G}$ are the second-order sensitivities of modeled O_3 to global (i.e., across the entire domain) NO_x and VOC emissions, respectively, and $S^2_{NOx-VOC,G}$ represents the second-order cross sensitivity to global NO_x and VOC emissions (also see Itahashi et al., 2020b).

3.1 Trends in Surface and Aloft O_3

Detailed comparison of simulated surface-level predictions of O_3 and related species over the 1990-2010 period from the hemispheric CMAQ model with available measurements from surface networks in the United States, Europe, and Asia have previously been reported in Xing et al. (2015) and are briefly summarized in Section S1 of the Supporting Information. Those results show that the model calculations were able to capture the significant and contrasting trends in surface-level O_3 distributions across the Northern Hemisphere suggested by the observations, with declining trends across North America and western Europe resulting from control measures on combustion-related sources and increases across large parts of Asia associated with economic and population growth. Additionally, the model performance statistics were comparable with results from other studies in regions across the Northern Hemisphere. Comparisons of trends in daily maximum 8-hour average O_3 ($DM8O_3$) with corresponding trends inferred from the Clean Air Status and Trends Network (CASTNET) measurements (Puchalski, 2021) further indicated that the model captured the spatial variability in the direction of the trends across the CASTNET sites, though the hemispheric model underestimated the magnitude of the trend (Mathur et al., 2017). Further examination of the CASTNET and simulated trends in $DM8O_3$ distributions during the 1990-2010 period are shown in Figure 2, which depicts the spatial variability in trends (estimated as the slope of the linear regression) in the lower percentiles of the spring-time (March-April-May) $DM8O_3$ distributions across a portion of the model domain covering the United States at the surface and for model layers at altitudes around 1.5 km and 3.2 km above ground-level, nominally representing the upper parts of the daytime planetary boundary layer and the lower free troposphere, respectively. Increases in 5^{th} and 25^{th} percentile surface-level $DM8O_3$ are noticed at many sites (filled circles in Figure 2a and 2d) both in the western and eastern United States and are similar to those reported in other prior studies (e.g., Cooper et al., 2012). These increases in lower percentile $DM8O_3$ likely result from a combination of reduced O_3 titration associated with declining NO_x emissions and

subsequent transport of higher O_3 to rural areas as well as possible increases in baseline O_3 resulting from increases in larger-scale regional and hemispheric tropospheric O_3 values. Similar increases are also captured in the HCMAQ multidecadal simulations for this period, though the magnitude of the trend is underestimated. The underestimation in part results from uncertainties in global emission estimates and their changes as well as coarse model grid resolution (Mathur et al., 2017; Section S1.1 in Supporting Information). The increasing contributions of long-range transport to tropospheric O_3 across the western United States is less ambiguous in the modeled DM8O_3 trends at 1.5 km (Figures 2b and 2e) and 3.2 km (Figures 2c and 2f), altitudes at which trends in O_3 distributions are largely driven by regional and hemispheric scale transport. Using backward sensitivity calculations with the CMAQ-Adjoint model (Hakami et al., 2007) that quantitatively link surface-level and aloft pollution, Mathur et al. (2018) show that at many locations across the U.S. more than 80% of sensitivity of ground-level O_3 is controlled by O_3 in layers aloft between 200-2000m. Consequently, it can be expected that downward entrainment of this increased free-tropospheric ozone contributes to the modeled (and by inference observed) increasing trends in the lower percentile DM8O_3 at the surface and point to the need to better characterize the contributions of emissions from different source regions to the changing amounts of the O_3 reservoir aloft.

3.2 Source-Region Contributions to O_3

To elucidate the spatially varying influence of emissions from different regions to O_3 distributions across the Northern Hemisphere, Figure 3(b-h) present the estimated fractional contributions inferred from the sum of the individual sensitivities to NO_x and VOC emissions from each region following Equation 4. In constructing this figure, we first averaged computed hourly sensitivities over the entire season (March-April-May) and for all model layers between the surface and 2 km and refer to these as planetary boundary layer (PBL) and seasonal average values in subsequent discussions. The ratio of the first order sensitivity for a source region, i, (or the stratosphere) to the sum of all first-order sensitivities (or fraction f_i) can be viewed to approximately represent the relative importance of the different emission source regions and the stratosphere in shaping the O_3 distributions in the lower troposphere across the Northern Hemisphere as:

$$f_i = \frac{\overline{S}_i}{\left(\sum_{j=1}^{N} \left(\overline{S}_{\mathrm{NO}_x,j} + \overline{S}_{VOC,j}\right) + \overline{S}_{\mathrm{STE}}\right)} \tag{5}$$

where, N is the number of geographic regions and the overbars denote average values over the season and for all model layers between the surface and 2km. Figure 3a presents the simulated PBL-average O_3 distribution for Spring 2006 across the Northern Hemisphere and Figures 3(b-i) illustrate the fractional contributions of the tracked sources and illustrate the relative importance of the different emission source regions and the stratosphere in shaping the O_3

distributions in the lower troposphere across the Northern Hemisphere. Similar illustrations of the model estimated source signatures for the other seasons (Summer, Winter, and Fall) are presented in the supplemental information (Figure S6-S8). These figures illustrate that O_3 produced from precursor emissions in a continent can undergo long range transport and impact tropospheric composition across vast remote oceans as well as far downwind continental regions. This intercontinental transport is more prominent during Spring and Summer with pronounced signatures of trans-Pacific transport of O_3 from East Asia and trans-Atlantic transport of O_3 from North America. During Spring and Summer, O_3 attributable to emissions in East Asia undergoes long-range transport and can contribute several percent of the estimated imported O_3 pollution across vast regions of continental North America. Emissions from Central America can also influence boundary-layer O_3 mixing ratios over large portions of the Southwestern United States. Also evident in Figures 3 and S7 is the dominant contribution (>50% of the total first-order O_3 sensitivity) of STE processes in dictating PBL O_3 abundance across the Northern Hemisphere during Spring and Winter when the height of the tropopause is lower and the stratospheric influence can penetrate far into the lower troposphere (e.g., Elbern et al., 1998; Wang et al., 2002; Langford et al., 2012; Lin et al., 2012; Xing et al., 2016; Mathur et al., 2017; Itahashi et al., 2020a). The widespread signature of the STE sensitivity depicted in these figures supports the notion that stratospheric impacts on lower tropospheric O_3 are not limited only to deep intrusion events. Air masses advected into a region are also influenced by STE process upwind, resulting in the broad spatial signature of estimated STE contributions depicted in these illustrations. This highlights the need, in background O_3 assessment and attribution analysis, for improved quantification of the amount of O_3 in surface air that is attributable to stratospheric O_3.

3.3 Estimates of O_3 Imported to the North American Troposphere

While the terminology "background pollution" has traditionally been used to represent air pollution that is not produced locally, in context of ground-level O_3 assessments, several definitions of background O_3 now appear in literature and largely depend on the geographic extent of the region considered, on the distinction between controllable and non-controllable portions of the O_3 imported to the region of interest, and whether O_3 production from precursors emitted from natural sources (e.g., wildfires, biogenic, STE) are considered (see Jaffe et al., 2018). To avoid confusion, for the purpose of this study we use the term "imported O_3" to represent the non-local contribution to the pollution in a region, and thus define it as the concentration attributable to sources (natural or anthropogenic) outside of the geographic region of interest. Following this definition, and the design of our sensitivity calculations described in section 2, we can estimate the imported O_3 for any geographic region, m, (defined in Section 2 and depicted in Figure 1) as the sum of the first-order sensitivities of all sources other than m as follows

$$O_{3_m}^{\text{imported}} = \sum_{j \neq m} \left(\overline{S}_{\text{NO}_x,j} + \overline{S}_{VOC,j} \right) + \overline{S}_{\text{STE}}. \quad (6)$$

Note that this imported O_3 plus the O_3 attributable to natural emissions of precursors (wildfires, vegetation, soil, lightning) from within a region has been used in some studies to estimate the background O_3 for a region (e.g., Emery et al., 2012; Fiore et al., 2014; Dolwick et al., 2015).

Following the definition in Equation (6), Figure 4 illustrates the estimated seasonal average O_3 for Spring and Summer of 2006 over a region encompassing the United States and surrounding portions of Canada and Mexico that can be attributed to transport from the stratosphere and all other source regions across the Northern Hemisphere other than NAM. Figure 4a and 4b present the spatial variations across this region for average values between the surface and 2 km, for Spring and Summer (seasons with typically higher tropospheric O_3), respectively, while Figures 4c and 4d show similar values for the model surface layer. Similar estimates for the cooler season (Winter) are presented in Figure S9 in the supplemental information. Significant spatial and seasonal variations are noted in the estimated imported O_3 mixing ratios, with higher values in the high elevation regions of the western United States. The estimated imported O_3 levels are higher during Spring than during Summer. Even though photochemical O_3 production is highest in Summer leading to higher localized regional O_3, long-range transport and STE are more prominent during Spring, leading to the higher Spring imported (and background) O_3 values. Additionally, the estimated imported O_3 values for the model's surface layer are lower than the estimated 0-2 km average because of O_3 removal at the surface due to dry deposition and titration by surface NO_x emissions, highlighting the need for adequate vertical resolution in large scale models, not only to better represent long-range transport but also processes influencing ground-level O_3.

To further shed light on the relative contributions of the various source regions across the Northern Hemisphere on the estimated imported O_3 values illustrated in Figure 4, we examined the relative contributions of the source regions to these estimated values. Figure 5 illustrates the fractional contributions of the six emission source regions and the stratosphere to the estimated average 0-2 km Spring imported O_3 across the United States, while Figure 6 presents similar estimates for Summer. During Spring, cross-Pacific transport of O_3 originating from Asia is estimated to contribute 10-20% of the O_3 imported to the lower troposphere over North America. Transport from Central America also accounts for comparable fractions (and up to 30%) of the imported O_3 in the south-central and southwestern states. Coastal regions across the western, eastern, and southern shores of the United States also show a persistent 10-20% contribution from sources across the vast oceanic regions of the Northern Hemisphere (represented by OTH or other), indicating the important role of emissions from the open ocean commercial shipping sector on tropospheric O_3 distributions and transport to downwind continents. The largest contribution to imported O_3 in the lower troposphere during Spring is estimated to be from O_3 that is of stratospheric origin with fractional contributions ranging between 29-78% across the continental United States. High-latitude regions typically show greater influence of STE (Figure 5g) and the fractional contributions are

much higher during Spring and Winter (refer to Figure S10 in supplemental information) when height of the tropopause is lower (e.g., Elbern et al., 1998) and the stratospheric influence can penetrate far down to the lower troposphere. Contrasting Figures 5, 6, and S10, it is also apparent that the relative contributions of the different sources to imported (and thus background) O_3 vary seasonally and are dictated by prevalent large-scale flow patterns. Notably during Summer, even though the estimated imported O_3 values are comparatively lower, they are influenced to a larger extent by source regions in closer proximity as indicated by the larger fractional contributions from Central America and the ocean region. Nevertheless, the role of cross tropopause transport of O_3 (i.e., STE) is seen to be a significant contributor to the non-local or imported O_3 budget in most seasons and is further illustrated in Figure 7 which presents spatial distributions across the contiguous U.S. and surrounding portions of the estimated contributions of stratospheric O_3 to seasonal mean surface-2km average O_3 mixing ratios for Spring and Summer. The magnitude and spatial variability of stratospheric O_3 inferred from the DDM-3D sensitivities are comparable to prior brute-force estimates reported in Xing et al. (2016) and Mathur et al. (2017). Additionally, as reported in Itahashi et al. (2020a) the interpretation of STE events as represented by the O_3-PV correlation in the model, is not strongly influenced by the model's horizontal grid resolution since the WRF meteorological model employs assimilation of analyzed meteorological fields in the UTLS. Consequently, the estimated PV fields in the UTLS and the representation of STE events are similar across the different resolutions. Highest amounts of stratospheric O_3 are seen in the high elevation locations of the western U.S. with significantly higher values during Spring compared to summer as also suggested by the fractional contributions illustrated in Figures 5g and 6g. As suggested by our results, both the amounts and fractions vary spatially and seasonally in response to the tropopause height, and perhaps even more episodically, from deep intrusion events associated with weather patterns and frontal movement. Our estimated STE fractional contributions are comparable with estimates presented in Roelofs and Lelieveld (1997), who, using a global chemistry-transport model, estimated that stratospheric contributions to surface O_3 varied between 10-60% depending on season and location. Since our estimates represent STE contributions to the imported O_3 to the North American troposphere and excludes the locally produced amounts, the estimated 29-78% range is expectedly higher. Tightening O_3 NAAQS and decreasing amounts of photo-chemically derived O_3 due to continuously declining anthropogenic precursor emissions across large parts of North America, further emphasize the need for accurately characterizing this fraction of O_3 in the troposphere, especially at the surface, that is of stratospheric origin. Finally, it should be noted that the fractional contributions of the different source regions to the estimated imported O_3 for the 0-2 km altitude average are relatively similar to the fractional contributions for the surface (contrast Figures 5 and S11) even though the absolute imported O_3 mixing ratios at the surface are lower (Figure 4). This is because non-local O_3 at the surface largely originates from the long-range transported O_3 aloft (e.g., Mathur et al., 2018).

3.4 Trends in Long-Range Transported O_3

Observations from a variety of in-situ and space-borne platforms have suggested that the global tropospheric O_3 burden has increased over the past several decades (Gaudel et al., 2018). Impacts of changes in anthropogenic emissions, particularly increases in East and South Asia and decreases in North America and Europe, on regional and global tropospheric O_3 burden have been assessed through modeling analysis (e.g., Xing et al. 2015, Zhang et al., 2021). These spatially heterogeneous changes in O_3 precursor emissions are not only modulating the tropospheric O_3 budget, but also likely altering long-range transport patterns and contributions at distant receptor regions. To investigate the impact of these contrasting changes in NO_x and VOC emissions across the Northern Hemisphere over a multi-decadal period on long-range transported O_3 and the changing source region contributions, we formulated a reduced-form model combining the detailed sensitivity calculations analyzed in preceding sections with previously conducted HCMAQ simulations for the 1990-2010 period. The reduced form model utilizes three key pieces of information from these detailed model calculations: (1) sensitivity coefficients for the base year 2006, (2) emission changes for each source region for each year during the 1990-2010 period relative to the base year (estimated on a regional aggregate and seasonal basis), and (3) three-dimensional O_3 distributions simulated by HCMAQ for the 1990-2010 period as described in Xing et al. (2015).

The long-range-transported O_3 to a region m from all other emission source regions for the base year (i.e., 2006) can be estimated as the sum of the zero-out contributions from all regions other than m following Equation 6 as:

$$C^{\text{base}}_{LRT,\ m} = \sum_{j \neq m} \left(\overline{S}_{\text{NO}_x,j} + \ \overline{S}_{VOC,j} \right). \tag{7}$$

Note that the definition of long-range transported O_3 above is equivalent to the imported O_3 (estimated by Equation 6) without the STE contribution. Given the perturbations in regional-total emissions for a specific year relative to the base year, we can estimate the specific perturbation year concentrations for year N (C^N_{est}) using the first-order sensitivities in the Taylor series approximation as

$$C^N_{\text{est}} = \ C^{\text{base}} + \ \sum \left(\overline{S}_{\text{NO}_x,j} \ \ \varepsilon^N_{\text{NO}_x,j} + \ \overline{S}_{VOC,j} \ \ \varepsilon^N_{VOC,j} \right). \tag{8}$$

Following the above equations, the long-range transported contributions to a region m in the perturbation year can then be approximated as

$$C^N_{LRT,m} = C^{\text{base}}_{LRT,m} + \sum_{j \neq m} \left(\overline{S}_{\text{NO}_x,j} \ \ \varepsilon^N_{\text{NO}_x,j} + \ \overline{S}_{VOC,j} \ \ \varepsilon^N_{VOC,j} \ \right) \tag{9}$$

Substituting Equation (7) in Equation (9) yields,

$$C^N_{LRT,m} = \sum_{j \neq m} \left(\overline{S}_{\mathrm{NO}_x,j} \; + \; \overline{S}_{VOC,j} \; \right) + \sum_{j \neq m} \left(\overline{S}_{\mathrm{NO}_x,j} \; \varepsilon^N_{\mathrm{NO}_x,j} + \; \overline{S}_{VOC,j} \; \varepsilon^N_{VOC,j} \; \right)$$

$$= \sum_{j \neq m} \left(\overline{S}_{\mathrm{NO}_x,j} \; E^N_{\mathrm{NO}_x,j} + \; \overline{S}_{VOC,j} \; E^N_{VOC,j} \; \right) \tag{10}$$

where $E^N_{\mathrm{NO}_x,j} = 1 + \; \varepsilon^N_{\mathrm{NO}_x,j}$ and $E^N_{VOC,j} = 1 + \; \varepsilon^N_{VOC,j}$.

Note that since we did not explicitly track the sensitivity to initial conditions, boundary conditions, O_3 production from methane (which currently is a prescribed global value), higher order sensitivities for each individual source region, and since the computed single-year sensitivity coefficients cannot represent impacts of possible changes in year-to-year meteorology, the reconstructed O_3 field using a Taylor series approximation will not precisely match the modeled O_3 field. To normalize for this discrepancy and to incorporate impacts of year-to-year meteorological variability on the seasonal average estimates, we scale the year-specific long-range transported estimates by the ratio of the modeled O_3 mixing ratio for the specific year (C^N) to its reconstructed value (C^N_{recon}) as detailed in Equations 11-12 below:

$$C^N_{LRT,m} = \left(\sum_{j \neq m} \left(\overline{S}_{\mathrm{NO}_x,j} \; E^N_{\mathrm{NO}_x,j} + \; \overline{S}_{VOC,j} \; E^N_{VOC,j} \; \right) \right) \left(\frac{C^N}{C^N_{\mathrm{recon}}} \right) \tag{11}$$

where,

$$C^N_{\mathrm{recon}} \approx \; C^{\mathrm{base}} + \sum \left(\overline{S}_{\mathrm{NO}_x,j} \; \varepsilon^N_{\mathrm{NO}_x,j} + \; \overline{S}_{VOC,j} \; \varepsilon^N_{VOC,j} \right) + \overline{S}_{\mathrm{STE}} + \frac{1}{2!} \overline{S}^{\,2}_{\mathrm{NO}_x,\;\;G} \left(\varepsilon^N_{\mathrm{NO}_x,G} \right)^2 + \frac{1}{2!} \overline{S}^{\,2}_{\mathrm{VOC}_G} \left(\varepsilon^N_{VO}$$

Recall that in Equation 12, $S^2_{NOx,G}$, $S^2_{VOC,G}$ and $S^2_{NOx-VOC,G}$ are the second order sensitivities to domain-wide NO_x and VOC emissions, and $\varepsilon^N_{\mathrm{NO}_x,G}$ and $\varepsilon^N_{VOC,G}$ represent the change in domain wide NO_x and VOC emissions, respectively for year N relative to 2006. It may also be noted that the estimated C^N_{recon} values are typically within 6% of the C^N for majority of the grid cells across the Contiguous U.S. as further detailed in section S3 in the Supporting Information.

Based on the reduced form model encapsulated by Equations 11-12, one can then estimate the long-range transported O_3 to a specific region (defined in

Figure 1) that is attributable to O_3 originating from all other source regions for each year of the 21-year analysis period of 1990-2010. Figure 8 illustrates the distribution and changes in this long-range transported O_3 across the United States for Spring; Figures 8a-c illustrate the estimated long-range transported amounts for the specific years of 1990, 2000 and 2010 while Figure 8d illustrates the change in this long-range transported O_3 depicted as the trend expressed in ppb/yr over the 21-years spanning 1990-2010. Figure S12 presents similar estimates for changes in long-range transported O_3 for Summer. All values shown in Figures 8 and S12 are computed from 0-2 km average mixing ratios. As illustrated in Figures 8 and S12, the amount of long-range transported O_3 to North America has steadily increased during the 1990-2010 period both during Spring and Summer. Several ppb of O_3 within the boundary layer across the continental United States can be attributed to this long-range transport during both seasons. In general, long-range transport contributions to boundary layer and surface O_3 are larger in the western and south-western states, which also show greater rates of increase in such influences over this time-period. Though not directly comparable due to differences in time-periods, averaging periods and metrics examined, the estimated magnitude of the trend across portions of the Western United States are comparable to those suggested in prior measurement and modeling studies (Cooper et al., 2012; Nopmongcol et al., 2016; Gaudel et al., 2018).

To further examine the changing influences of the different source regions to long-range transported O_3 to North America, Figure 9 depicts the seasonal mean contributions during Spring for the years 1990 and 2010, contrasting conditions at the start and end of our analysis period. Figure 10 further illustrates the changes in the relative contributions of the various source regions during the 1990-2010 period. In constructing this figure, we examined the contribution of each source region to the estimated long-range transported O_3 at each model grid cell within the region shown in Figures 8 and S12. To illustrate the changing contributions of these source regions to the long-range transported O_3 we plot the changes in the median value of these contributions across all these grid cells over the 21-year time-period in Figure 10.

Collectively, Figures 8-10 reveal several important features of long-range transported O_3 to North America: (1) changes in LRT O_3 during the 1990-2010 periods across the continental United States vary spatially and so do the contributions from the different source regions, (2) the relative contributions of the different source regions to LRT O_3 vary seasonally and have changed (and will likely continue to change) in response to spatially heterogeneous changes in anthropogenic precursor emissions across the globe, (3) cross-Atlantic transport of Europe's contributions have steadily declined (median contributions from ~30% in 1990 to 13% in 2010) in response to reductions in NO_x and VOC emissions in that region, (4) O_3 attributable to emissions in East and South-east Asia is a dominant contributor (median values from 25-38%) to LRT O_3, with increasing contributions over the 1990-2010 period associated with increasing emissions in the region, (5) emissions from Central America also contribute a sizeable

fraction of the imported O_3 across portions of the south western United States (greater than 3 ppb on seasonal mean basis), (6) O_3 attributable to emissions from the large oceanic regions across the Northern Hemisphere (large fraction of the OTH in Figure 1) has also been a significant contributor to LRT O_3, with a distinct increasing contribution (median contributions up to 32%) in recent years, (7) emissions from sources in closer proximity to North America (i.e., Central America and the Oceans) expectedly have a larger contribution to O_3 imported to the North American troposphere during Summer and contribute to the noted higher values of LRT O_3 in Summer relative to Spring (contrast Figures 8a-c and S12a-c).

Noticeable in Figures 9 and 10 is the prominent and increasing contribution of O_3 in the North American troposphere attributable to emissions from the source region marked OTH in Figure 1, which is largely comprised of the vast oceanic regions of the Northern Hemisphere. NO_x emissions from this region predominantly result from marine transportation activities. Though shipping is considered a relatively energy efficient mode for transportation of goods, NO_x emissions from shipping are relatively high, because most marine engines operate at high temperatures and pressures without effective reduction technologies. Oceangoing ships are estimated to contribute around 15% of all global anthropogenic NO_x emissions and an increase in international ship traffic has raised concerns about possible impacts of their emissions on tropospheric composition, climate effects, and health impacts (Dalsøren et al., 2009; Hoor et al., 2009; Eyring et al., 2010; Sofiev et al., 2018; Zhang et al., 2021). Analyzing results from global and regional model calculations, Jonson et al. (2020) found that the largest contribution to ozone in several regions and countries in Europe was from sea areas well outside European waters associated with open sea shipping. Using a source tagging method in a global chemical transport model, Butler et al. (2002) estimated 2-5ppb contribution of shipping NO_x emissions to annual mean surface O_3 across North America with larger values during Spring in the northwestern U.S. While the magnitude of our estimated contributions from shipping emissions over North America are slightly lower than those reported in Butler et al. (2020), they do show similar widespread impacts over downwind continental regions. Figure 11 presents the changes in NO_x emissions associated with this sector during our analysis period as estimated in the EDGAR inventory used in our model calculations. Evident from Figure 11 is the steady increase in emissions (~60% during 1990-2010) from this sector associated with an increase in international transportation of goods and commercial trading, highlighting the role of increasing NO_x emissions from shipping on the tropospheric O_3 burden and its increasing contributions to O_3 imported to North America during the 1990-2010 period as illustrated in Figure 10. These results emphasize the need for more accurate characterization of the spatial and temporal variability in NO_x emissions from ships across the vast oceanic regions to better help guide policies seeking reductions in emissions from this sector that effectively offset the anticipated growth in seaborne trade.

1. Summary and Conclusions

Significant and contrasting changes in emissions of tropospheric O_3 precursor species have and continue to occur across the globe in response to implementation of control measures and changes in patterns of emission producing activities. These changes are not only impacting the local O_3 levels and distributions that are sensitive to these emissions, but also influencing the large-scale distribution of O_3 across the global troposphere. Since the lifetime of O_3 in the free troposphere, depending on altitude, can vary from several days to a month, once produced and lofted to the free troposphere, it can be efficiently transported inter-continentally (e.g., NRC, 2009; TFHTAP, 2010). Increasing amounts of long-range transported O_3 impact background levels in receptor regions and confound development and implementation of local abatement strategies to manage pollution and mitigate effects on human and ecological health. Analysis of long-term measurements of O_3 (e.g., Chang et al., 2017; Gaudel et al., 2018) highlight these changing trends in its distributions across the globe. However, since measurements represent the cumulative impacts of multiple atmospheric dynamical-chemical-physical process on emissions from a multitude of source regions, measurements alone are unable to unambiguously attribute the causes of the noted trends to emissions from a source region or uniquely differentiate contributions from intercontinental transport relative to those from STE.

Employing multi-decadal model simulations of the changes in tropospheric O_3 distributions across the Northern Hemisphere from a comprehensive atmospheric modeling system in conjunction with detailed sensitivity calculations characterizing the response of tropospheric O_3 to NO_x and VOC emissions from source regions across the Northern Hemisphere, we estimate that on a seasonal-mean basis, during the 1990-2010 period, LRT O_3 to regions across the Continental United States steadily increased by 0.06-0.2 ppb yr^{-1} in response to changes in precursor emissions outside North America. This net trend, in turn, arises from superposition of unequal and contrasting trends in contributions from different emission source regions across the Northern Hemisphere. Both the amount of long-range transported O_3 and the magnitude of its trend vary spatially and are larger in the western United States than those in the east. Even though the inferred relative contributions of the different source regions over this multi-decadal period exhibit inter-annual variability, they provide valuable information on the seasonal variations in these contributions as well as the changing relative importance of their emissions to the long-range transported O_3 to North America. Specifically, the model calculations show that declining emissions in Western Europe have substantially reduced its contributions to LRT O_3 across the United States; median values of the estimated contributions declined from ~30% in the early 1990's to ~15% in 2010. In contrast, cross-Pacific transport of O_3 attributable to Asian emissions contributed 20-35% of the estimated LRT O_3 with an increasing trend during 1990-2010, as also suggested in several prior modeling studies analyzing impacts of perturbations in Asian emissions (e.g., Jacob et al., 1999; Fiore et al., 2009). On a seasonal basis, the contributions of O_3 originating from emissions in the Indian subcontinent are comparatively small throughout the analysis period.

This is consistent with results in Butler et al. (2020) that also show that impact of emissions from South Asia is relatively localized and their transport does not influence hemispheric background to the same extent as O_3 produced from other source regions in the Northern Hemisphere. Emissions from Central America are shown to modulate O_3 levels across portions of southwestern United States with median contributions to LRT O_3 across the United States varying between 5-15% across seasons and years. Also, since O_3 production is more efficient during warmer periods, sources in closer proximity to the United States, specifically Central America and shipping emissions, exhibit higher contributions during summer compared to other seasons.

Highlighted by our analysis is the prominent and increasing contribution of emissions from shipping operations across the vast oceans. Though the impacts of shipping emissions on air quality in ports and coastal areas across the world have been frequently studied, and the role of SO_2 (and consequently aerosol sulfate) and carbon dioxide (CO_2) from the sector as modulators of global climate is well acknowledged, the prominent contribution of NO_x emissions from the sector to large-scale O_3 distributions and subsequent impacts on background O_3 in downwind continents is only recently being recognized (e.g., Jonson et al., 2018; Mertens et al., 2018; Butler et al., 2020; Jonson et al., 2020). It should be noted that limited field measurements of ship plume chemical composition, suggest that instantaneous dilution of ship emissions over coarse gird volumes may overestimate ozone production in vicinity of ship emissions (e.g., Chen et al., 2005) and are thus suggested to represent upper limits over the ocean basins (Butler et al., 2020). While ship plume parameterizations in large scale models improved model estimated concentrations in the vicinity of the source relative to measurements of the first few of hours of aging they exhibited minor differences in simulated ozone over downwind continental regions (e.g., Vinken et al., 2011) suggesting that the effects of the parameterizations on grid resolved chemistry and estimated far field impacts are small. This could be because across the more variable conditions of the open oceans, some fraction of the ship NO_x survives beyond the plume parameterization aging (e.g., von Glasow et al., 2003; Holmes et al., 2014) which along with NO_x sequestered in reservoir species (e.g., organic nitrates), in addition to shipping NO_x transported longer distances nocturnally, then impact grid resolved chemistry and the subsequent estimated far field impacts. For instance, in their source tagging simulations Butler et al. (2020) found that significant amount of PAN is formed downwind of regions in which anthropogenic VOCs are emitted, often via reaction with NO_x emitted from shipping. Though both the horizontal resolution and vertical layer spacing used in our model calculations is much finer than most large-scale models, as in many global models (Eyring et al., 2007; Butler et al., 2020; Jonson et al., 2020), we neglect plume dilution due to a lack of consensus and availability of robust parameterizations in common modeling systems. As noted in Butler et al. (2020), future work exploring optimal grid resolution to minimize impacts of artificial ship plume dilution would be useful. Nevertheless, our results reveal that LRT O_3 attributable to emissions

from shipping has increased in response to the steadily increasing NO_x emissions from the sector as captured in the EDGARv4.2 emission inventory used in our model calculations. During the 2005-2010 period and perhaps even in the contemporary atmosphere, the contributions of shipping emissions to O_3 imported to the U.S. troposphere are comparable to those from transport of O_3 attributable to East Asian emissions and suggest possibly even higher contributions in the future if NO_x emissions from commercial shipping operations were to increase in response to anticipated growth in seaborne trade (Eyring et al., 2010). Future studies could utilize detailed information on ship type and position from Automatic Identification Systems (AIS) transponders to better characterize spatial and temporal variability in shipping emissions (e.g., Jalkanen et al., 2012). This combined with finer horizontal resolution simulations would enable not only improved quantification of shipping emissions but potentially also improved representation of the chemistry in ship exhaust plumes both in the vicinity of the ship tracks but also as they are transported to downwind continental regions.

In addition to the O_3 attributable to emissions from the source regions across the Northern Hemisphere, model calculations also suggest that air masses entering the North American domain have sizeable contributions of O_3 that is of stratospheric origin. In context of our model set up and calculations, the sum of the LRT O_3 and that attributable to STE represent the amount of O_3 originating from sources other than emissions within the domain and thus representative of the non-local or "imported" O_3 levels. The modeled sensitivities to O_3 resulting from STE processes indicate large contributions to boundary layer and ground-level O_3, the magnitude of which is consistent with prior brute force estimates (Xing et al., 2016; Mathur et al., 2018). Our estimates suggest that O_3 that is of stratospheric origin could constitute 29-78% of the estimated Spring background O_3 across the continental United States; high-latitude regions typically show greater influence of STE. Additionally, since comparisons of HCMAQ predictions with ozonesonde measurements indicate a systematic low bias in free-troposphere O_3 mixing ratios (e.g., Hogrefe et al., 2018), the estimated STE modeled contributions to boundary-layer O_3 may be considered conservative. Nevertheless, the widespread spatial signature of the sensitivity to modeled O_3 resulting from STE processes noted for all seasons, and especially Spring and Winter when the tropopause height is lower, supports the notion that stratospheric impacts on lower tropospheric and ground-level O_3 are not limited only to deep intrusion events. Air masses advected into a region are also influenced by STE process upwind, resulting in the noted broad spatial signature of estimated STE contributions. This highlights the need for improved quantification of the variability and amount of O_3 in surface air that is attributable to the stratosphere in background O_3 assessments and estimation.

Our results show that the intercontinental transport of pollutants has and continues to change in response to emission changes across the globe. Accurately quantifying the impacts of changes in emissions in distant continents on amounts of pollution imported is becoming as important as domestic control measures at

receptor continents. Analyzing the impact of well documented and contrasting multi-decadal (1990-2010) changes in emissions across the Northern Hemisphere helped better explain the dominant source regions that drive the noted changes in observed O_3 mixing ratios across the United States and highlight the need for greater emphasis on reducing uncertainties in emissions associated with commercial shipping and in characterization of space and time variability in lower tropospheric O_3 that is of stratospheric origin. While our analyses have focused on better understanding factors influencing long-range transport of O_3 to North America and portions of the United States, the existing calculations and the reduced form model could easily be extended to any of the other continental source regions defined in Figure 1. Though our analyses focused on O_3, many of the issues discussed here are also applicable to other criteria pollutants (e.g., $PM_{2.5}$), and any potential actions taken to understand or reduce background O_3 may also reduce background concentrations of other pollutants.

1. Caveats and Future Directions

Changes in O_3 precursor emissions across the globe have occurred during the decade post our 1990-2010 analysis period and have likely further altered tropospheric O_3 distributions and amounts transported intercontinentally. Based on review of the current state of knowledge, Jaffe et al. (2018) summarize estimates of seasonal U.S. background O_3 (USB O_3) to be 20-40 ppb depending on location with an uncertainty of $\pm$10 ppb. While our estimates are within the reported range, our methodology could be refined further for current time periods by leveraging recent enhancements to the HCMAQ modeling system and its evolving applications. In particular, enhancements to the representation of seasonal variations in the impacts of (1) halogen chemistry in marine environments (Sarwar et al., 2019), (2) stratosphere-troposphere exchange (Xing et al., 2016; Mathur et al., 2017), and (3) emissions from natural sources such as lightning NO_x (Kang et al., 2020) will enable more accurate representation of seasonal changes in attribution of the source regions in terms of absolute O_3 mixing ratios. These model process enhancements combined with updates in global emission estimates and trends for the contemporary atmosphere are currently being used to simulate changes in tropospheric composition across the Northern Hemisphere during 2002-2017 as part of EPA's Air Quality Time Series (EQUATES) project (Foley et al., 2020). A refined DDM-3D configuration that explicitly tracks O_3 sensitivities to natural sources plus anthropogenic sources in countries outside the United States could then be deployed to estimate attributions commensurate with the U.S. background (USB) O_3 definition (i.e., influence of all sources other than U.S. anthropogenic emissions (Dolwick et al., 2015)) used in policy deliberations. These simulations could also help quantify the impact of recent emission reductions in East Asia (e.g., Zheng et al., 2018) on cross-Pacific transport of O_3. In addition, expanding the set of sensitivity coefficients to also include sensitivity to initial and boundary conditions, and second-order sensitivity to NO_x emissions from individual countries would enable more accurate attribution of absolute O_3 mixing ratio contributions for the 2002-2017 period, extending the reduced form model framework

developed in this study. As computational resources increase and model efficiency improves, multi-year DDM-3D calculations could also be conducted to more robustly assess possible impacts of meteorological variability on inferred long-range transport impacts of the different source regions. Multi-year average sensitivity coefficients may also yield a more robust reduced form model to project the impacts of future emission changes. The current analyses focused on regionally aggregate changes in emissions, and thus represents response to average emission changes over large geographic source regions. New features in CMAQ that allow disaggregation of input emissions (Murphy et al., 2021), in conjunction with explicit tracking of sensitivity to the sector emissions can facilitate developing inferences on impacts of changes in emissions from specific sectors if desired.

Code and Data Availability: CMAQ source code is freely available via https://github.com/usepa/cmaq.git. Archived CMAQ versions are available from the same repository. Data used to generate figures shown in this article are available from Mathur (2021). The raw model outputs are available upon request from the corresponding author. Observational data from the CASTNET network (Puchalski, 2021) are available at: https://www.epa.gov/castnet .

Acknowledgements: We thank Wyat Appel, Terry Keating, and Norm Possiel for constructive comments and suggestions on initial versions of this manuscript.

Disclaimer: The views expressed in this paper are those of the authors and do not necessarily represent the view or policies of the U.S. Environmental Protection Agency.

Notes: The authors declare no competing financial interest.

References

Jacob, D. J., J. A. Logan, and P. P. Murti (1999), Effect of rising Asian

emissions on surface ozone in the United States, Geophys.Res.Lett.,

26(14), 2175–2178, doi:10.1029/1999GL900450

Jacob, D. J., J. A. Logan, and P. P. Murti (1999), Effect of rising Asian

emissions on surface ozone in the United States, Geophys.Res.Lett.,

26(14), 2175–2178, doi:10.1029/1999GL900450

American Lung Association (ALA), State of the air 2020, https://www.stateoftheair.org/assets/SOTA-2020.pdf [accessed 26 May 2021].

Butler, T., Lupascu, A., and Nalam, A. (2020). Attribution of ground-level ozone to anthropogenic and natural sources of nitrogen oxides and reactive carbon in a global chemical transport model, Atmos. Chem. Phys., 20, 10707–10731. https://doi.org/10.5194/acp-20-10707-2020

Chameides, W.L., Kasibhatla, P.S., Yienger, J. and Levy II, H. (1994). Growth of Continental-Scale Metro-Agro-Plexes, Regional Ozone Pollution, and World

Food Production. *Science*, 264, 74-77. DOI: 10.1126/science.264.5155.74

Chang, K.-L., Petropavlovskikh, I., Cooper, O.R., Schultz, M.G., Wang, T. (2017). Regional trend analysis of surface ozone observations from monitoring networks in eastern North America, Europe and East Asia. *Elem. Sci. Anth.*, 5: 50. DOI: https://doi.org/10.1525/elementa.243

Chen, G., Huey, L., Trainer, M., Nicks, D., Corbett, J., Ryerson, T., Parrish, D., Neuman, J., Nowak, J., Tanner, D., Holloway, J., Brock, C., Crawford, J., Olson, J., Sullivan, A., Weber, R., Schauffler, S., Donnelly, S., Atlas, E., Roberts, J., Flocke, F., Hübler, G., and Fehsenfeld, F. (2005). An investigation of the chemistry of ship emission plumes during ITCT 2002, J. Geophys. Res., 110, D10S90. doi:10.1029/2004JD005236

Cohan, D. S., Hakami, A., Hu, Y. T., and Russell, A. G. (2005). Nonlinear response of ozone to emissions: Source apportionment and sensitivity analysis. *Environ. Sci. Technol.*, 39, 6739–6748. https://doi.org/10.1021/es048664m

Cohan D.S., Napelenok S.L. (2011). Air Quality Response Modeling for Decision Support, *Atmosphere*, 2(3), 407-425. https://doi.org/10.3390/atmos2030407

Cooper, O. R., et al. (2010). Increasing springtime ozone mixing ratios in the FT over western North America, *Nature*, 463(7279), 344–348. doi:10.1038/nature08708

Cooper, O.R., Gao, R-S. Tarasick, D., Leblanc, T., Sweeney, C. (2012). Long-term ozone trends at rural ozone monitoring sites across the United States, 1990-2010. *J. Geophys. Res.*,117, D22307. doi:10.1029/2012JD018261

Cromar, K.R., Gladson, L.A., and Ewart, G. (2019). Trends in Excess Morbidity and Mortality Associated with Air Pollution above American Thoracic Society-Recommended Standards, 2008-2017. *Ann Am Thorac Soc.*, 16(7):836-845. doi: 10.1513/AnnalsATS.201812-914OC

Dalsøren, S. B., Eide, M. S., Endresen, Ø., Mjelde, A., Gravir, G., and Isaksen, I. S. A. (2009). Update on emissions and environmental impacts from the international fleet of ships: the contribution from major ship types and ports. *Atmos. Chem. Phys.*, 9, 2171–2194, https://doi.org/10.5194/acp-9-2171-2009.

Dolwick, P., Akhtar, F., Baker, K. R., Possiel, N., Simon, H., and Tonnesen, G. (2015), Comparison of background ozone estimates over the western United States based on two separate model methodologies, *Atmos. Environ.*, 109, 282–296.

Elbern, H., Hendricks, J., and Ebel, A. (1998). A climatology of tropopause folds by global analyses. *Theor. Appl. Climatol.*, 59, 181–200. https://doi.org/10.1007/s007040050023.

Emery, C., Jung, J., Downey, N., Johnson, J., Jimenez, M., Yarwood, G., Morris, R. (2012). Regional and global modeling estimates of policy relevant background

ozone over the United States, *Atmos. Environ.*, 47, 206e217. http://dx.doi.org /10.1016/j.atmosenv.2011.11.012.

European Commission: Joint Research Centre (JRC)/Netherlands Environmental Assessment Agency. Emission Database for Global Atmospheric Research (EDGAR), release version 4.2., available at: http://edgar.jrc.ec.europa.eu, 2011.

Eyring, V., Stevenson, D. S., Lauer, A., Dentener, F. J., Butler, T., Collins, W. J., Ellingsen, K., Gauss, M., Hauglustaine, D. A., Isaksen, I. S. A., Lawrence, M. G., Richter, A., Rodriguez, J. M., Sanderson, M., Strahan, S. E., Sudo, K., Szopa, S., van Noije, T. P. C., and Wild, O. (2007). Multi-model simulations of the impact of international shipping on Atmospheric Chemistry and Climate in 2000 and 2030, Atmos. Chem. Phys., 7, 757–780. http://www.atmos-chem-phys.net/7/757/2007/

Eyring, V., Isaksen, I. S. A., Berntsen, T., Collins, W. J., Corbett J. J., Endresen, Ø., Grainger, R. G., Moldanova, J., Schlager, H., and Stevenson, D. S. (2010). Transport Impacts on Atmosphere and Climate: Shipping. *Atmos. Environ.*, 44, 4735–4771. https://doi.org/10.1016/j.atmosenv.2009.04.059

Fiore, A. M., et al. (2009). Multimodel estimates of intercontinental source-receptor relationships for ozone pollution. *J. Geophys. Res.*, 114, D04301. doi:10.1029/2008JD010816

Fiore, A.M., Oberman, J.T., Lin, M., Zhang, L., Clifton, O.E., Jacob, D.J., Naik, V., Horowitz, L.W., Pinto, J.P., Milly, G.P. (2014). Estimating North American background ozone in U.S. surface air with two independent global models: variability, uncertainties, and recommendations, *Atmos. Environ.* 96, 284e300. http://dx.doi.org/10.1016/j.atmosenv.2014.07.045

Foley, K. et al. (2020). EQUATES: EPA's Air Quality Time Series project, presented at the 19$^{\text{th}}$ Annual CMAS Conference, available at: https://cmascenter.org/conference/2020/slides/KFoley_EQUATES_CMAS_2020.pdf.

Galmarini, S., Koffi, B., Solazzo, E., Keating, T., Hogrefe, C., Schulz, M., Benedictow, A., Griesfeller, J. J., Janssens-Maenhout, G., Carmichael, G., Fu, J., and Dentener, F. (2017). Technical note: Coordination and harmonization of the multi-scale, multi-model activities HTAP2, AQMEII3, and MICS-Asia3: simulations, emission inventories, boundary conditions, and model output formats. *Atmos. Chem. Phys.*, 17, 1543–1555. https://doi.org/10.5194/acp-17-1543-2017

Gaudel, A., Cooper, O. R., Ancellet, G., Barret, B., Boynard, A., Burrows, J. P., et al. (2018). Tropospheric Ozone Assessment Report: Present-day distribution and trends of tropospheric ozone relevant to climate and global atmospheric chemistry model evaluation. *Elementa: Science of the Anthropocene*, *6*, 39. https://doi.org/10.1525/elementa.291

Guenther, A., Hewitt, C. N., Erickson, D., Fall, R., Geron, C., Graedel, T., Harley, P., Klinger, L., Lerdau, M., McKay, W. A., Pierce, T., Scholes, B., Steinbrecher, R., Tallamraju, R., Taylor, J., and Zimmerman, P. (1995). A

Global Model of Natural Volatile Organic Compound Emissions, J. Geophys. Res., 100, 8873–8892.

Haagen-Smit, A. J. and Fox, M. M. (1954). Photochemical Ozone Formation with Hydrocarbons and Automobile Exhaust. Air Repair, 4, 3, 105-136. doi:10.1080/00966665.1954.10467649

Hakami, A., Odman, M.T., and Russell, A.G. (2003). High-order, direct sensitivity analysis of multidimensional air quality models. *Environ. Sci. Technol.*, 37, 2442–2452. https://doi.org/10.1021/es020677h

Hakami, A., Henze, D.K., Seinfeld, J.H., Singh, K., Sandu, A., Kim, S., Byun, D., Li, Q. (2007). The adjoint of CMAQ. *Environ. Sci. & Technol.*, 41, 7807-7817.

Hogrefe, C., Liu, P., Pouliot, G., Mathur, R., Roselle, S., Flemming, J., Lin, M., and Park, R. J. (2018). Impacts of different characterizations of large-scale background on simulated regional-scale ozone over the continental United States. *Atmos. Chem. Phys.*, 18, 3839–3864. https://doi.org/10.5194/acp-18-3839-2018

Hoor, P., Borken-Kleefeld, J., Caro, D., Dessens, O., Endresen, O., Gauss, M., Grewe, V., Hauglustaine, D., Isaksen, I. S. A., Jöckel, P., Lelieveld, J., Myhre, G., Meijer, E., Olivie, D., Prather, M., Schnadt Poberaj, C., Shine, K. P., Staehelin, J., Tang, Q., van Aardenne, J., van Velthoven, P., and Sausen, R. (2009). The impact of traffic emissions on atmospheric ozone and OH: results from QUANTIFY, Atmos. Chem. Phys., 9, 3113–3136. https://doi.org/10.5194/acp-9-3113-2009

Itahashi, S., Mathur, R., Hogrefe, C., and Zhang, Y. (2020a). Modeling stratospheric intrusion and trans-Pacific transport on tropospheric ozone using hemispheric CMAQ during April 2010 – Part 1: Model evaluation and air mass characterization for stratosphere–troposphere transport, *Atmos. Chem. Phys.*, 20, 3373–3396, https://doi.org/10.5194/acp-20-3373-2020.

Itahashi, S., Mathur, R., Hogrefe, C., Napelenok, S.L. and Zhang, Y. (2020b). Modeling stratospheric intrusion and trans-Pacific transport on tropospheric ozone using hemispheric CMAQ during April 2010 – Part 2: Examination of emission impacts based on the higher-order decoupled direct method. *Atmos. Chem. Phys.*, 20, 3397–3413. https://doi.org/10.5194/acp-20-3397-2020

Jacob, D. J., Logan, J.A. and Murti, P.P. (1999). Effect of rising Asian emissions on surface ozone in the United States. *Geophys. Res. Lett.*, 26(14), 2175–2178. doi:10.1029/1999GL900450.

Jaffe, D., et al. (1999). Transport of Asian air pollution to North America. *Geophys. Res. Lett.*, 26(6), 711–714. doi:10.1029/1999GL900100.

Jaffe, D., Price, H., Parrish, D., Goldstein, A., and Harris, J. (2003). Increasing background ozone during spring on the west coast of North America. *Geophys. Res. Lett.*, 30(12), 1613. doi:10.1029/2003GL017024

Jaffe, D.A., Cooper, O.R., Fiore, A.M., Henderson, B.H., Tonnesen, G.S., Russell, A.G., Henze, D.K., Langford, A.O., Lin, M., and Moore, T. (2018). Scientific assessment of background ozone over the U.S.: Implications for air quality management. *Elem Sci Anth*, 6, 56. DOI: https://doi.org/10.1525/elementa.309

Jalkanen, J.-P., Johansson, L., Kukkonen, J., Brink, A., Kalli, J., and Stipa, T. (2012). Extension of an assessment model of ship traffic exhaust emissions for particulate matter and carbon monoxide, Atmos. Chem. Phys., 12, 2641–2659. https://doi.org/10.5194/acp-12-2641-2012

Jonson, J. E., Schulz, M., Emmons, L., Flemming, J., Henze, D., Sudo, K., Tronstad Lund, M., Lin, M., Benedictow, A., Koffi, B., Dentener, F., Keating, T., Kivi, R., and Davila, Y. (2018). The effects of intercontinental emission sources on European air pollution levels. *Atmos. Chem. Phys.*, 18, 13655–13672. https://doi.org/10.5194/acp-18-13655-2018.

Jonson, J. E., Gauss, M., Schulz, M., Jalkanen, J.-P., and Fagerli, H. (2020). Effects of global ship emissions on European air pollution levels, Atmos. Chem. Phys., 20, 11399–11422. https://doi.org/10.5194/acp-20-11399-2020

Kang, D., Mathur, R., Pouliot, G. A., Gilliam, R.C., and Wong, D.C. (2020). Significant ground-level ozone attributed to lightning-induced nitrogen oxides during summertime over the Mountain West States, *Npj Clim. Atmos. Sci.*, 3, 6. https://doi.org/10.1038/s41612-020-0108-2

Krupa, S.V., Nosal, M., Legge, A.H. (1998). A numerical analysis of the combined open-top chamber data from the USA and Europe on ambient ozone and negative crop responses. *Environmental Pollution*, 101, 157-160. doi: 10.1016/s0269-7491(98)00019-0

Langford, A. O., Brioude, J., Cooper, O.R., Senff, C.J., Alvarez II, R.J., Hardesty, R.M., Johnson, B.J., and Oltmans, S.J. (2012). Stratospheric influence on surface ozone in the Los Angeles area during late spring and early summer of 2010, *J. Geophys. Res.*, 117, D00V06, doi:10.1029/2011JD016766

Lin, C., Jacob, D.J., Munger, W., and Fiore, A. (2000). Increasing background ozone in surface air over the United States. *Geophys. Res. Lett.*,27, 3465–3468, doi:10.1029/2000GL011762

Lin, M. Y., Fiore, A.M., Cooper, O.R., Horowitz, L.W., Langford, A.O., Levy, H., Johnson, B.J., Naik, V., Oltmans, S.J., and Senff, C.J. (2012). Springtime high surface ozone events over the western United States: Quantifying the role of stratospheric intrusions. *J. Geophys. Res.*, 117, D00v22. https://doi.org/10.1029/2012jd018151

Lin, M. Y., Horowitz, L.W. Payton, R., Fiore, A.M., Tonnesen, G. (2017). US surface ozone trends and extremes from 1980 to 2014: quantifying the roles of rising Asian emissions, domestic controls, wildfires, and climate. *Atmos. Chem. Phys.*, 17, 2943-2970. doi:10.5194/acp-17-2943-2017.

Lippman, M. (1993). Health-effects of tropospheric ozone – review of recent research findings and their implications to ambient air-quality standards. *J Expo Anal Env Epid* **3**(1): 103–129.

Mathur, R., Lin, H. M., McKeen, S., Kang, D., and Wong, D. (2008). Three-dimensional model studies of exchange processes in the troposphere: use of potential vorticity to specify aloft O3 in regional models. Presented at the 7th Annual CMAS Conference, available at: https://www.cmascenter.org/conference/2008/slides/mathur_three-dimension_model_cmas08.ppt.

Mathur, R., Xing, J., Gilliam, R., Sarwar, G., Hogrefe, C., Pleim, J., Pouliot, G., Roselle, S., Spero, T.L., Wong, D.C., Young, J. (2017). Extending the Community Multiscale Air Quality (CMAQ) modeling system to hemispheric scales: overview of process considerations and initial applications. *Atmos. Chem. Phys.*, 17, 12449-12474. https://doi.org/10.5194/acp-17-12449-2017

Mathur, R., Hogrefe, C., Hakami, A., Zhao, S., Szykman, J., and Hagler, G. (2018). A call for an aloft air quality monitoring network: need, feasibility, and potential value. *Environ. Sci. Technol.*, 52, 10903–10908, https://doi.org/10.1021/acs.est.8b02496

Mathur, R. (2021). Datasets for manuscript "How are Divergent Global Emission Trends Influencing Long-Range Transported Ozone to North America" [Data set]. U.S. EPA Office of Research and Development (ORD). https://doi.org/10.23719/1523043

Mertens, M., Grewe, V., Rieger, V. S., and Jöckel, P. (2018). Revisiting the contribution of land transport and shipping emissions to tropospheric ozone, Atmos. Chem. Phys., 18, 5567–5588. https://doi.org/10.5194/acp-18-5567-2018

Murphy, B. N., Nolte, C. G., Sidi, F., Bash, J. O., Appel, K. W., Jang, C., Kang, D., Kelly, J., Mathur, R., Napelenok, S., Pouliot, G., and Pye, H. O. T. (2021). The Detailed Emissions Scaling, Isolation, and Diagnostic (DESID) module in the Community Multiscale Air Quality (CMAQ) modeling system version 5.3.2. *Geosci. Model Dev.*, 14, 3407–3420. https://doi.org/10.5194/gmd-14-3407-2021.

NRC (2009). Global sources of local pollution: an assessment of long-range transport of key air pollutants to and from the United States. National Academy Press, Washington, DC, USA. https://doi.org/10.17226/12743.

Napelenok, S.L., Cohan, D.S., Odman, M.T. and Tonse, S. (2008). Extension and evaluation of sensitivity analysis capabilities in a photochemical model. *Environ. Model. Softw.*, 23, 994–999. https://doi.org/10.1016/j.envsoft.2007.11.004

Nopmongcol, U., Jung, J., Kumar, N. and Yarwood, G. (2016). Changes in US background ozone due to global anthropogenic emissions from 1970-2020.

Atmos. Environ., 140, 446-455. http://dx.doi.org/10.1016/j.atmosenv.2016.06.026

Parrish, D.D., Dunlea, E.J., Atlas, E.L., Schauffler, S., Donnelly, S., Stroud, V., Goldstein, A.H., Millet, D.B., McKay, M., Jaffe, D.A., Price, H., Hess, P.G., Flocke, F., Roberts, J.M. (2004). Changes in the photochemical environment of the temperate North Pacific troposphere in response to increased Asian emissions. *J. Geophys. Res.*, 109, D23S18. doi:10.1029/2004JD004978.

Price, C., Penner, J., and Prather, M. (1997). NOx from lightning 1: Global distribution based on lightning physics, J. Geophys. Res., 102(D5), 5929–5941.

Puchalski, M. (2021). Clean Air Status Trends Network (CASTNET) Hourly Ozone Concentrations [Data set]. U.S. Environmental Protection Agency. https://doi.org/10.23719/1520792

Roelofs, G. J., and Lelieveld, J. (1997). Model study of the influence of cross-tropopause O_3 transports on tropospheric O_3 levels. *Tellus*, 49B, 38-55. https://doi.org/10.3402/tellusb.v49i1.15949

Sarwar, G., Gantt, B., Foley, K., Fahey, K., Spero, T. L., Kang, D., Mathur, R., Foroutan, H., Xing, J., Sherwen, T., and SaizLopez, A. (2019). Influence of bromine and iodine chemistry on annual, seasonal, diurnal, and background ozone: CMAQ simulations over the Northern Hemisphere. *Atmos. Environ.*, 213, 395– 404, https://doi.org/10.1016/j.atmosenv.2019.06.020

Simon, H, Reff, A, Wells, B, Xing, J and Frank, N. (2015). Ozone trends across the United States over a period of decreasing NOx and VOC emissions. *Environ Sci Technol.*, 49(1), 186–195. DOI: https://doi. org/10.1021/es504514z

Sofiev M, Winebrake J J, Johansson L, Carr E W, Prank M, Soares J, Vira J, Kouznetsov R, Jalkanen J P and Corbett J J. (2018) Cleaner fuels for ships provide public health benefits with climate tradeoffs, *Nat. Commun.*, 9, 1–12. https://doi.org/10.1038/s41467-017-02774-9

Task Force on Hemispheric Transport of Air Pollution (TFHTAP). (2010). Hemispheric Transport of Air Pollution, Part A: Ozone and Particulate Matter, edited by F. Dentener, T. Keating, and H. Akimoto, United Nations Publ. ECE/EB.AIR/100, U. N. Econ. Comm. for Eur. Inf. Serv., Geneva, Switzerland. [Available at www.htap.org].

Treves, K. and Rudich, Y. (2003). The atmospheric fate of C_3-C_6 hydroxyalkyl nitrates. *J. Phys. Chem. A,* 107 (39), 7809–7817. doi: 10.1021/jp035064l, 2003.

U.S. EPA. (2020a). Integrated Science Assessment (ISA) for Ozone and Related Photochemical Oxidants (Final Report, Apr 2020). U.S. Environmental Protection Agency, Washington, DC, EPA/600/R-20/012.

U.S. EPA. (2020b). National Air Quality: Status and Trends of Key Air Pollutants, https://www.epa.gov/air-trends.

von Glasow, R., Lawrence, M. G., Sander, R., and Crutzen, P. J. (2003). Modeling the chemical effects of ship exhaust in the cloudfree marine boundary layer, Atmos. Chem. Phys., 3, 233–250, doi:10.5194/acp-3-233-2003.

Wang, K.-Y., Shallcross, D.E. and Pyle, J.A. (2002). Seasonal variations and vertical movement of the tropopause in the UTLS region. *Ann. Geophys.*, 20, 871-874. doi:10.5194/angeo-20-871-2002.

Xing, J., Mathur, R., Pleim, J., Hogrefe, C., Gan, C., Wong, D.C., Wei, C., Gilliam, R., Pouliot, G. (2015). Observations and modeling of air quality trends over 1990-2010 across the northern hemisphere: China, the United States and Europe. *Atmos. Chem & Phys.*, 15, 2227-2914, doi:10.5194/acp-15-2723-2015.

Xing, J., Mathur, R., Pleim, J., Hogrefe, C., Wang, J., Gan, C.-M., Sarwar, G., Wong, D., and McKeen, S. (2016). Representing the effects of stratosphere-troposphere exchange on 3D O_3 distributions in chemistry transport models using a potential vorticity based parameterization. *Atmos. Chem. Phys.*, 16, 10865-10877, doi:10.5194/acp-16-10865-2016

Yang, Y.J., Wilkinson, J.G. and Russell, A.G. (1997). Fast, direct sensitivity analysis of multidimensional photochemical models. *Environ. Sci. Technol.*, 31, 2859–2868. https://doi.org/10.1021/es970117w

Zhang, Y., Eastham, S.D., Lau, A.K.H., Fung, J.C., and Selin, N.E. (2021). Global air quality and health impacts of domestic and international shipping, *Env. Res. Lett.*, 16. https://doi.org/10.1088/1748-9326/ac146b

Zhang, Y., West, J. J., Emmons, L. K., Flemming, J., Jonson, J. E., Lund, M.T., et al. (2021). Contributions of World Regions to the Global Tropospheric Ozone Burden Change from 1980 to 2010. *Geophysical Research Letters*, *48*, 2021. https://doi.org/10.1029/2020GL089184.

Zheng, B., Tong, D., Li, M., Liu, F., Hong, C., Geng, G., Li, H., Li, X., Peng, L., Qi, J., Yan, L., Zhang, Y., Zhao, H., Zheng, Y., He, K., and Zhang, Q. (2018). Trends in China's anthropogenic emissions since 2010 as the consequence of clean air actions, *Atmos. Chem. Phys.*, 18, 14095–14111, https://doi.org/10.5194/acp-18-14095-2018.

References From the Supporting Information

Bey, I., Jacob, D. J., Yantosca, R. M., Logan, J. A., Field, B., Fiore, A. M., Li, Q., Liu, H., Mickley, L. J., and Schultz, M. (2001). Global modeling of tropospheric chemistry with assimilated meteorology: Model description and evaluation, *J. Geophys. Res.*, 106, 23073–23096.

Colette, A., Granier, C., Hodnebrog, Ø., Jakobs, H., Maurizi, A., Nyiri, A., Bessagnet, B., D'Angiola, A., D'Isidoro, M., Gauss, M., Meleux, F., Memmesheimer, M., Mieville, A., Rouïl, L., Russo, F., Solberg, S., Stordal, F., and Tampieri, F. (2011). Air quality trends in Europe over the past decade: a first multi-model assessment, Atmos. Chem. Phys., 11, 11657–11678, doi:10.5194/acp- 11-11657-2011.

Donner, L.J. et al. (2011), The Dynamical Core, Physical Parameterizations, and Basic Simulation Characteristics of the Atmospheric Component AM3 of the GFDL Global Coupled Model CM3, *J. Climate*, 24, 3484–3519, https://doi.org/10.1175/2011jcli3955.1

Flemming, J., Huijnen, V., Arteta, J., Bechtold, P., Beljaars, A.,Blechschmidt, A.-M., Diamantakis, M., Engelen, R. J., Gaudel, A., Inness, A., Jones, L., Josse, B., Katragkou, E., Marecal, V., Peuch, V.-H., Richter, A., Schultz, M. G., Stein, O., and Tsikerdekis, A. (2015). Tropospheric chemistry in the Integrated Forecasting System of ECMWF, *Geosci. Model Dev.*, 8, 975–1003, https://doi.org/10.5194/gmd-8-975-2015.

Gan, C.-M., J. Pleim, R. Mathur, C. Hogrefe, C. N. Long, J. Xing, D. Wong, R. Gilliam, and C. Wei (2015). Assessment of long-term WRF–CMAQ simulations for understanding direct aerosol effects on radiation "brightening" in the United States, Atmos. Chem. Phys., 15, 12193-12209, doi:10.5194/acp-15-12193-2015.

Parrish, D. D., R. G. Derwent, W. Steinbrecht, R. Stübi, R. Van Malderen, M. Steinbacher, et al. (2020), Zonal similarity of long-term changes and seasonal cycles of baseline ozone at northern mid-latitudes. *J. Geophys. Res.: Atmos.,* 125, e2019JD031908, https://doi.org/10.1029/2019JD031908 doi: 10.1029/2019JD031908.

Wang, K., Zhang, Y., Jang, C., Phillips, S., and Wang, B.: Modeling intercontinental air pollution transport over the trans-Pacific region in 2001 using the Community Multiscale Air Quality modeling system, J. Geophys. Res.-Atmos., 114, D04307, doi:10.1029/2008JD010807, 2009.

Zhang, Y., Vijayaraghavan, K., Wen, X.-Y., Snell, H. E., and Jacobson, M. Z.: Probing into regional ozone and particulate matter pollution in the United States: 1. A 1 year CMAQ simulation and evaluation using surface and satellite data, J. Geophys. Res., 114, D22304, doi:10.1029/2009JD011898, 2009.

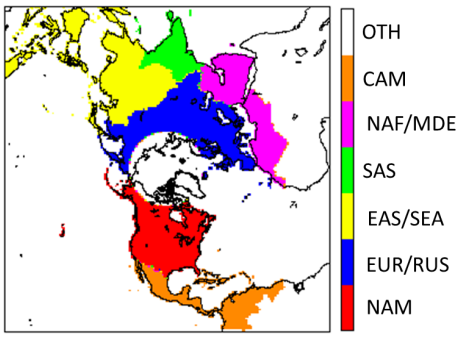

Figure 1: The Northern Hemisphere modeling domain and source region def-

inition: (1) North America (NAM), (2) Europe and Russia (EUR+RUS), (3) East and Southeast Asia (EAS+SEA), (4) South Asia (SAS; the Indian subcontinent), (5) Northern Africa and the Middle East (NAF+MDE), (6) Central America (CAM), and (7) The rest of the geographic domain (OTH).

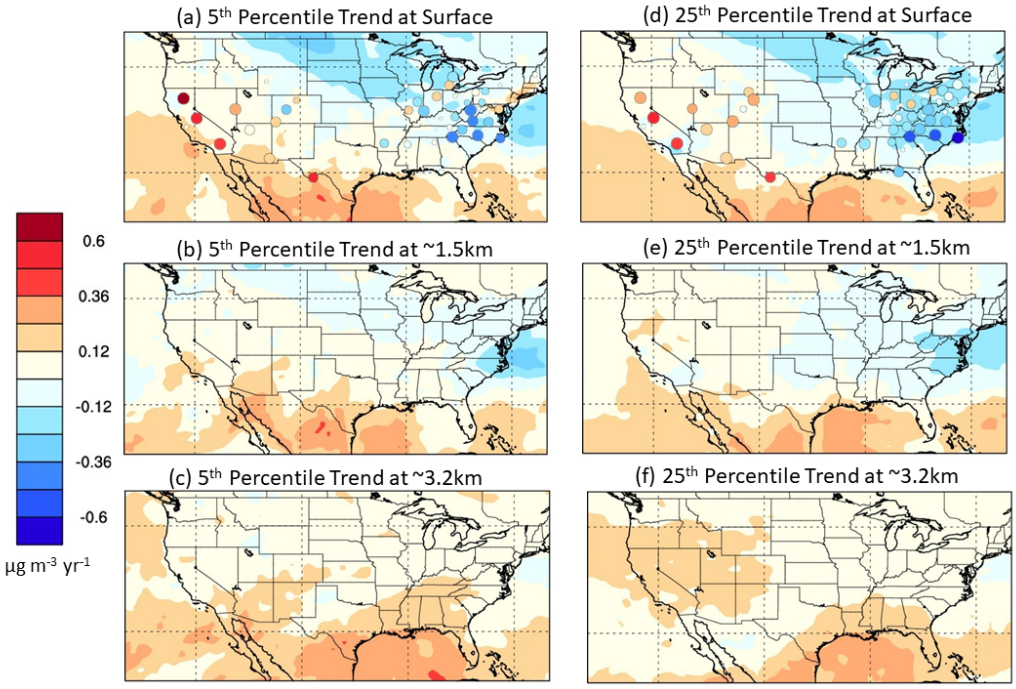

Figure 2: 1990-2010 trends in Spring (March-April-May) seasonal-average daily-maximum 8-hour-average O_3 ($DM8O_3$) distributions across a portion of the model domain covering the United States at the surface and at model layers at altitudes of 1.5 km and 3.2 km above ground-level. (a)-(c): trends in 5^{th} percentile $DM8O_3$ at different altitudes. (d)-(f): trends in 25^{th} percentile $DM8O_3$ at different altitudes. Filled circles in (a) and (d) represent corresponding observed trends at the CASTNET monitoring locations.

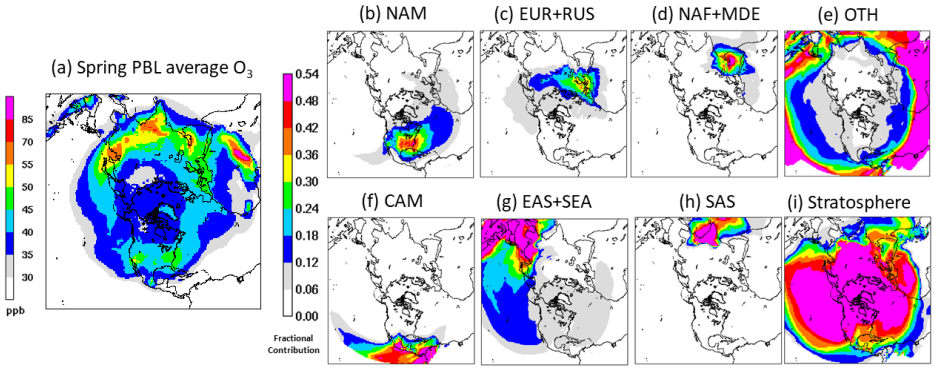

Estimated contributions of different source regions to O_3 distributions across the Northern Hemisphere. (a) PBL average O_3 during spring 2006. Fractional contributions of individual source regions: (b) NAM, (c) EUR+RUS, (d) NAF+MDE, (e) Other, (f) CAM, (g) EAS+SEA, (h) SAS and (i) stratosphere

Figure 3: Estimated contributions of different source regions to O_3 distributions across the Northern Hemisphere for Spring (March-April-May) 2006. (a) PBL average O_3 during spring 2006. Fractional contributions of individual source regions estimated from the first-order sensitivities: (b) NAM, (c) EUR+RUS, (d) NAF+MDE, (e) Other, (f) CAM, (g) EAS+SEA, (h) SAS and (i) stratosphere.

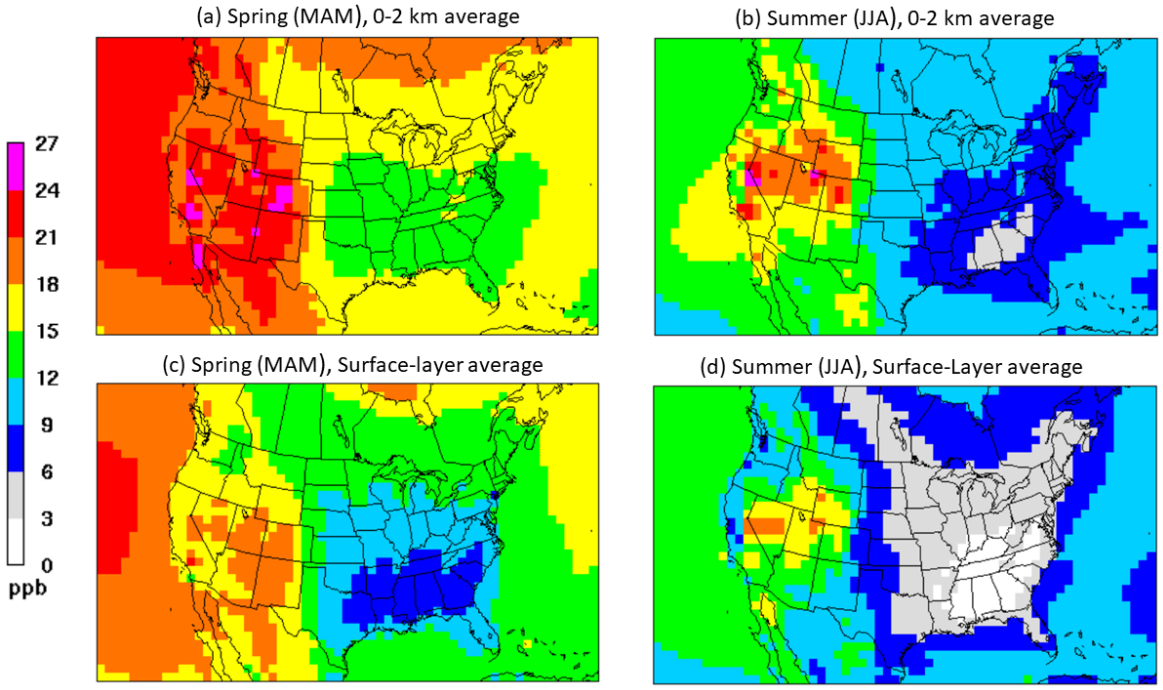

Figure 4: Estimated imported O_3 (defined as O_3 attributed to transport from the stratosphere and all other source regions across the Northern Hemisphere other than NAM) distributions across the United States and surrounding regions for the surface to 2km average for (a) Spring 2006 and (b) Summer 2006. (c) and (d) illustrate similar distributions but for the model's surface-layer.

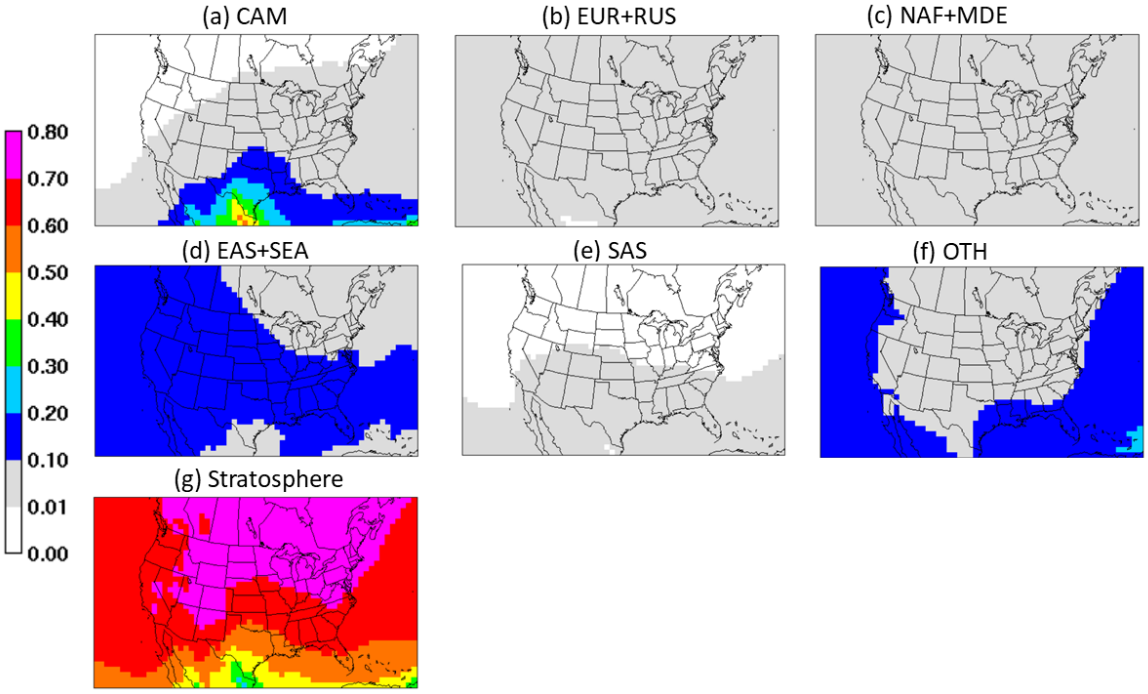

Figure 5: Fractional contributions of the different source regions to the 0-2km average Spring 2006 estimated imported O_3 mixing ratios in Figure 4a.

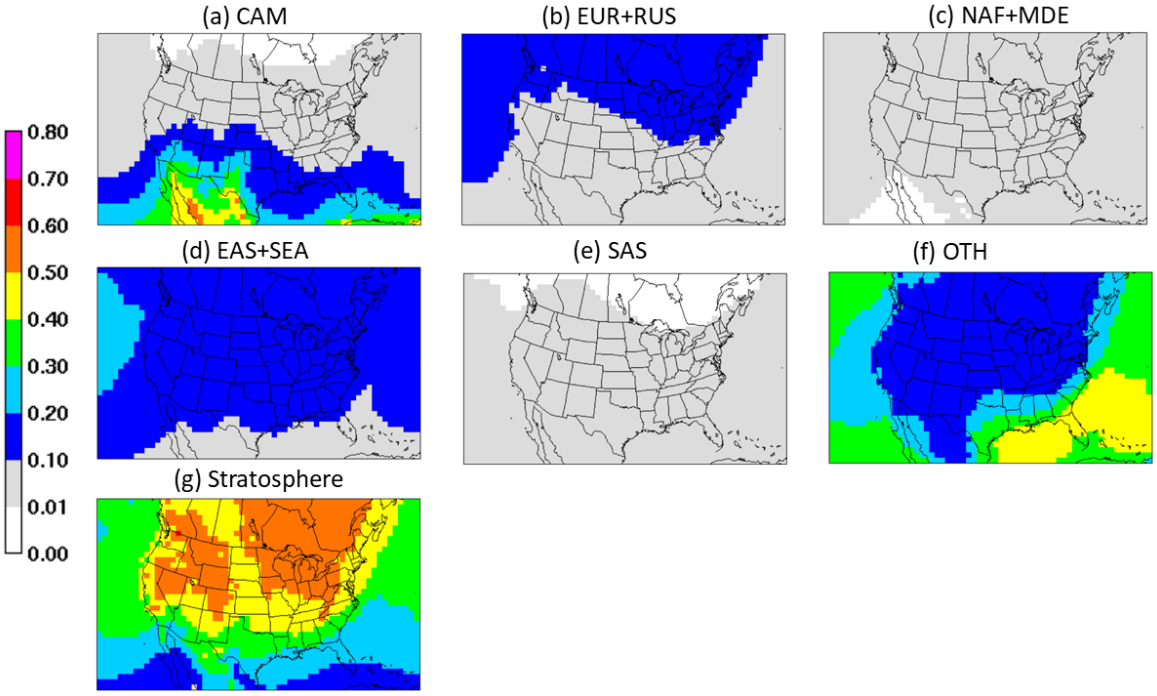

Figure 6: Fractional contributions of the different sources to the 0-2km average Summer 2006 estimated imported O_3 mixing ratios in Figure 4b.

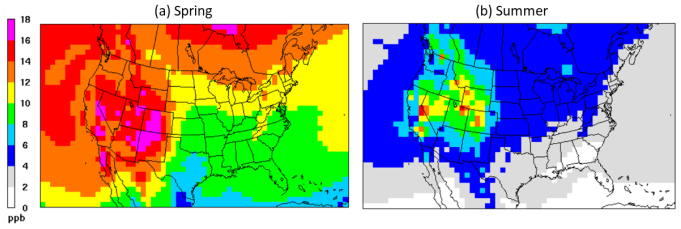

Estimated contributions of stratospheric O3 to seasonal-mean 0-2km average O3 mixing ratios during (a) Spring 2006, and (b) Summer 2006 (*add after fig6?*)

Figure 7: Estimated contributions of stratospheric O_3 to seasonal-mean 0-2km average O_3 mixing ratios for (a) Spring 2006 and (b) Summer 2006.

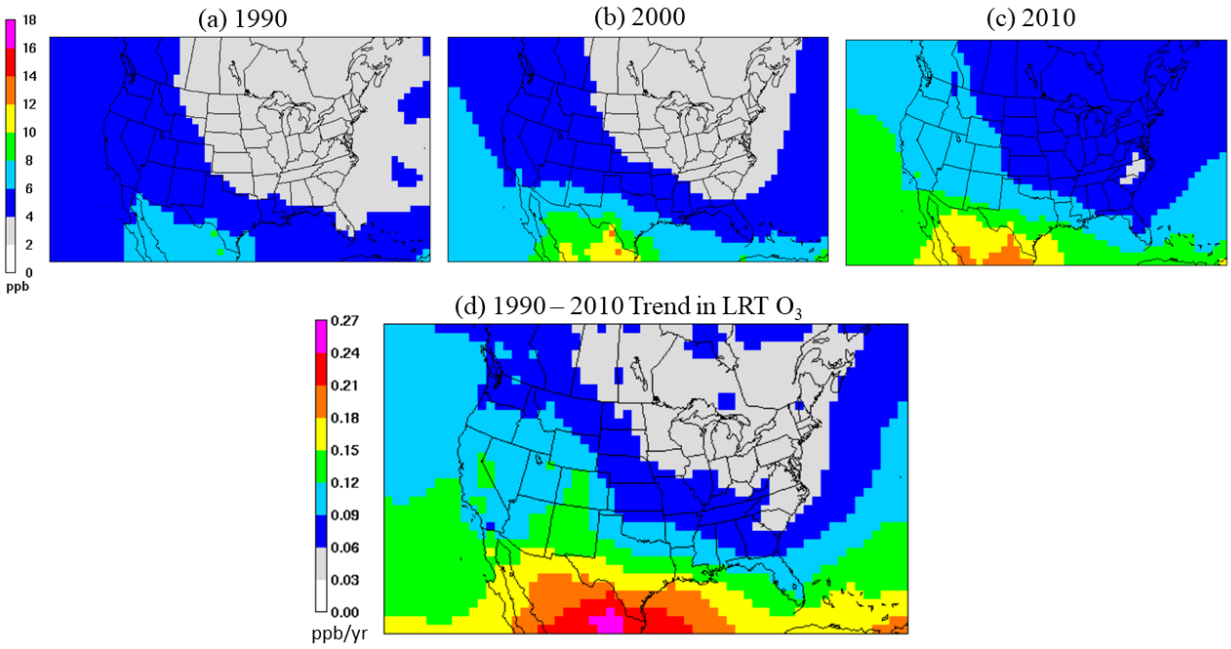

Figure 8: 1990-2010 changes in long-range transported O_3 to North America during Spring. Estimated long-range transported O_3 to North America from the different source regions for (a) 1990, (b) 2000, and (c) 2010. The estimated trend in long-range transported O_3 to North America for the 1990-2010 period is illustrated in (d). The trend is estimated as the slope of the linear regression of the estimated seasonal-mean long-range transported O_3 mixing ratios for each of the individual years in the 1990-2010 period. All estimates are for the 0-2km average O_3 mixing ratios.

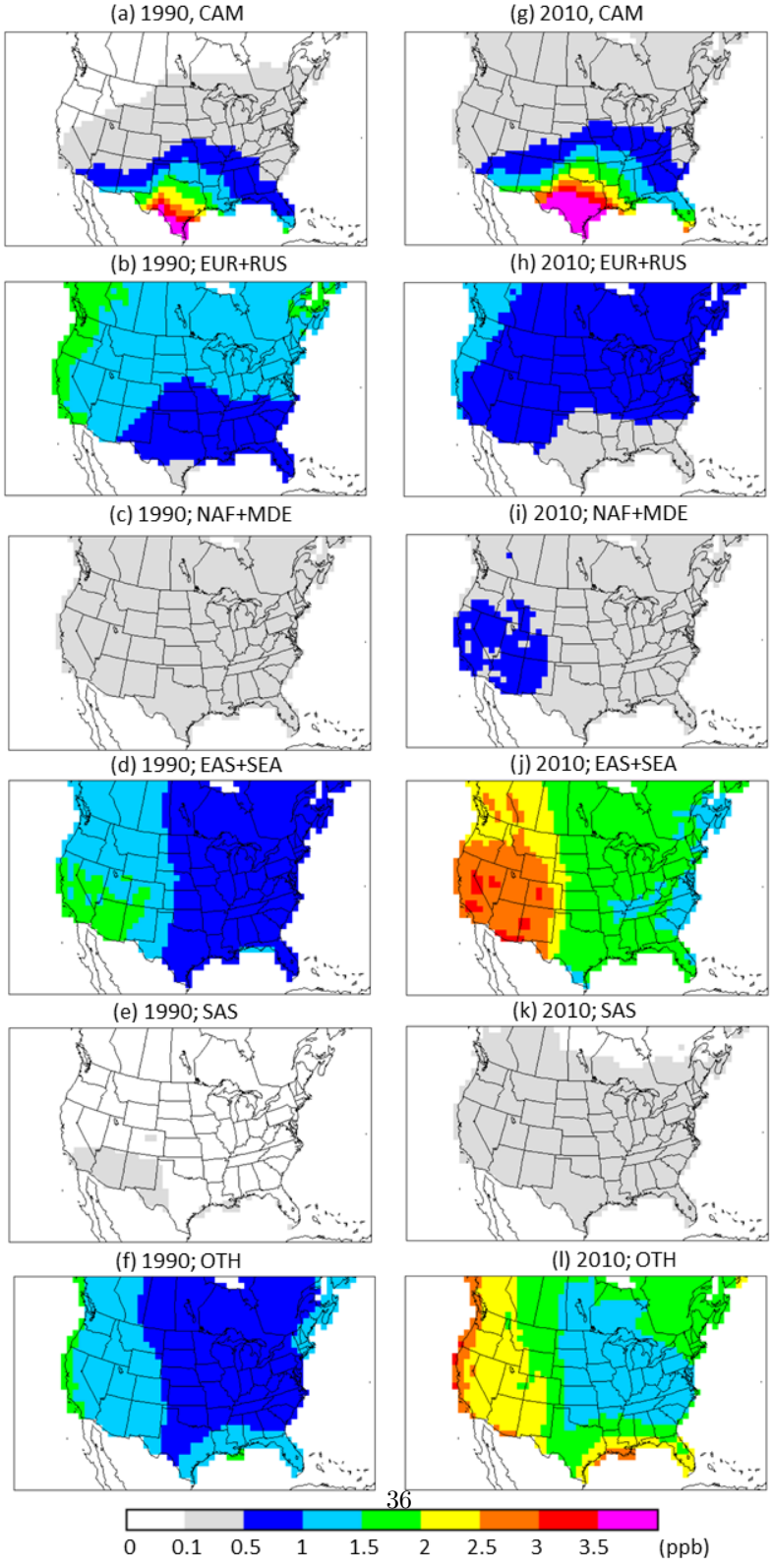
(a) 1990, CAM
(g) 2010, CAM
(b) 1990; EUR+RUS
(h) 2010; EUR+RUS
(c) 1990; NAF+MDE
(i) 2010; NAF+MDE
(d) 1990; EAS+SEA
(j) 2010; EAS+SEA
(e) 1990; SAS
(k) 2010; SAS
(f) 1990; OTH
(l) 2010; OTH
0 0.1 0.5 1 1.5 2 2.5 3 3.5 (ppb)

Figure 9: Estimated contributions of different source regions to long-range transported O_3 to North America during Spring for 1990 (a-f) and 2010 (g-l). All estimates are for the 0-2km average O_3 mixing ratios. Values are only shown for grid cells in the NAM region in Figure 1.

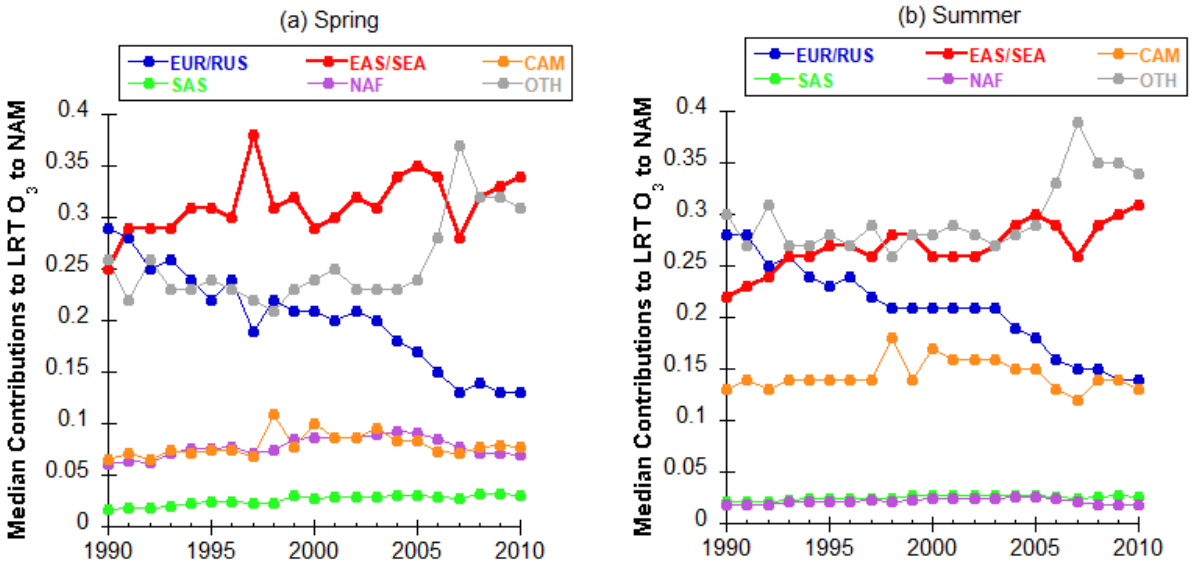

Figure 10: Changes in median fractional contributions to long-range transported O_3 to North America from different source regions during 1990-2010.

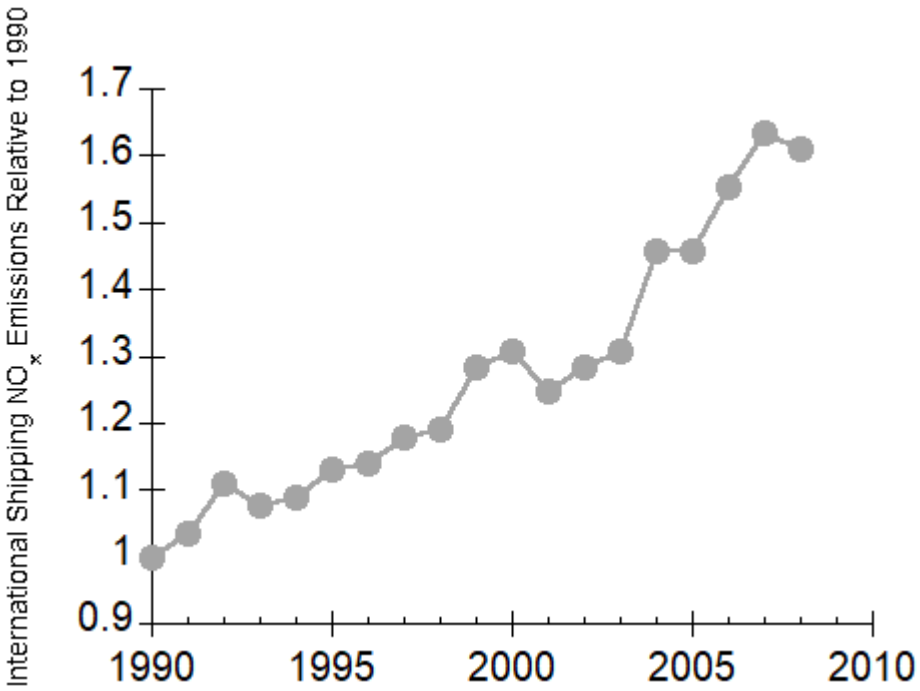

Figure 11: Changes in NO_x emissions from international shipping operations across the Northern Hemisphere during 1990-2008; Individual year emissions are normalized to the 1990 value.